COBIK
Center odličnosti za biosenzoriko, instrumentacijo in procesno kontrolo
Laboratorij za krmilne sisteme

Naložba v vašo prihodnost
Operacijo delno financira Evropska unija
Evropski sklad za regionalni razvoj

MODELLING OF FULLERENE PRODUCTION BY THE ELECTRIC ARC-DISCHARGE METHOD

Delovno poročilo: KM/2010/12, Verzija 1

Katarina Mramor
Nataša Grlj
Božidar Šarler

Ljubljana 2010

NAROČNIK:
COBIK
Center odličnosti za biosenzoriko, instrumentacijo in procesno kontrolo
Velika pot 22
SI-5250 Solkan

IZVAJALEC:
Laboratorij za krmilne sisteme
COBIK
Center odličnosti za biosenzoriko, instrumentacijo in procesno kontrolo
Velika pot 22
SI-5250 Solkan

NOSILEC NALOGE:
dr. Božidar Šarler, univ. dipl. fiz.

PROJEKT:
B.16: Računalniški model proizvodne celice

NASLOV POROČILA:
Modelling of fullerene production by the electric arc-discharge method

AVTOR POROČILA:
Katarina Mramor, univ. dipl. fiz.

ŠTEVILKA DELOVNEGA POROČILA:
KM/2010/12

LITERATURA:
Zbrana literatura se nahaja na portalu 4PM. V zavihku PORTALI: B.16 – Računalniški model proizvodne celice

Abstract

The molecules from fullerene family are rapidly becoming a part of our daily lives due to the wide range of their unique properties and extensive field of their potential applications. High demand for these materials revealed a necessity to understand the process of fullerene growth in order to optimize their production. Since the fabrication technique has a large influence on the material proper-ties, several methods have been suggested.

The focus of this seminar will be electric-arc discharge method, where fullerens are formed by vaporizing graphite electrodes in a low pressure gas atmosphere. Detailed understanding of growth mechanisms in the arc discharge reactor requires the development of a mathematical model that approximates the physical behaviour of nonequilibrium plasma coupled with nonlinear chemical systems.

In this seminar several such models from various authors ([1], [2], [3]) are presented along with chemical kinetics model [Scott, 2004], that describes nucleation and growth of carbon clusters and fullerens. In addition, a complementing literature review on the subject is performed. The majority of the contents in chapters 3, 4 and subchapters 5.1, 5.2 and 7.1 have been taken from the review of Nataša Grlj [4]. These chapters have been only slightly modified and complemented.

Contents

List of Symbols

a	constant
a_r	radial acceleration ($\frac{m}{s^2}$)
b	constant
c	free parameter
c_p	heat capacity at constant pressure ($\frac{kJ}{kgK}$)
d_{CNT}	distance (nm)
d_{NT-TN}	distance (nm)
e	electron charge (As)
$\vec{f}$	vector of body force per unit density ($\frac{m^4}{s^2}$)
$\vec{g}$	gravitational acceleration ($\frac{m}{s^2}$)
h	enthalpy ($\frac{kJ}{kg}$)
h_C	enthalpy of pure carbon($\frac{kJ}{mol}$)
h_g	enthalpy of buffer gas($\frac{kJ}{mol}$)
$\hat{i}$	unit vector in radial direction
$\hat{j}$	unit vector; angle measured counter clockwise from x axis
$\hat{k}$	unit vector in axial direction
$\vec{j}$	current intensity ($\frac{A}{m^2}$)
k	thermal conductivity ($\frac{W}{mK}$)
k_B	Boltzmann's constant ($\frac{kgm^2}{ks^2}$)
k_{1r}	forward rate constant of a reaction
k_{2r}	backward rate constant of a reaction
$\vec{n}$	normal vector
q_r	chemical reaction rate of progress ($\frac{1}{s}$)
$\vec{p}$	position vector (m)
$\vec{p}_i$	reference position vector (m)
r	radial distance between $\vec{p}$ and $\vec{p}_i$ (m)
r	radial coordinate (none)
s_{CR}	species production rate due to surface reactions ($\frac{mol}{m^2 s}$)
t	time (s)
$\vec{u}$	velocity vector ($\frac{m}{s}$)
u_A	gas velocity from the anode ($\frac{m}{s}$)
u_r	radial component of velocity vector ($\frac{m}{s}$)
u_z	axial component of velocity vector ($\frac{m}{s}$)
z	axis (none)
A	anode surface area (m^2)

$\vec{B}$	magnetic field intensity $(\frac{N}{Am})$
C_i	molar concentration of carbon species $(\frac{1}{s})$
D_C	diffusional coefficient of carbon species $(\frac{m^2}{s})$
D_{im}	diffusion coefficient matrix $(\frac{m^2}{s})$
D_{ji}	matrix of ordinal j multicomponent diffusion coefficients $(\frac{m^2}{s})$
D_i^T	thermal diffusion coefficient $(\frac{kg}{ms})$
$\vec{E}$	electric field $(\frac{V}{m})$
G	bulk growth rate $(\frac{m}{s})$
M_i	molecular weight $(\frac{kg}{mol})$
M_{CNT}	molecular weight of carbon nanotubes$(\frac{kg}{mol})$
N	number of points (none)
N_{at}	number of atoms per unit cell $(\frac{m}{s^2})$
N_{A_v}	Avogadro constant $(\frac{1}{mol})$
P	pressure $(\frac{N}{m^2})$
R	universal gas constant $(\frac{J}{molK})$
S_h	enthalpy source $(\frac{m}{s})$
S_{in}	negative source of species due to condensation $(\frac{m}{s})$
S_m	mass source $(\frac{m}{s})$
S_t	radiational loss per velocity $(\frac{m}{s})$
T	temperature (K)
T_A	anode temperature (K)
T_C	cathode temperature (K)
U	internal energy (J)
V	scaled radial velocity $(\frac{1}{s})$
V_i	species diffusion velocity $(\frac{m}{s})$
X_i	gas species mole fraction (none)
Y_C	carbon species mass fraction (none)
Y_i	gas species mass fraction (none)
Z_{CR}	surface species site fraction (none)
$\vec{\alpha}$	vector of expansion coefficients
α_i	expansion coefficient
ε	surface emissivity (none)
ε_n	net emission coefficient (J)
θ	data values corresponding to approximate function
μ	viscosity $(\frac{kg}{ms})$
ν_{ir}	stoichiometric coefficient of r-th reaction
$\nu_{ir}^{'}$	stoichiometric coefficient of r-th reactants for i-th reaction

ν''_{ir}	stoichiometric coefficient of r-th products for i-th reaction
ρ	mass density ($\frac{kg}{m^3}$)
ρ_{CNT}	nanotube bulk mass density ($\frac{kg}{m^3}$)
σ	electrical conductivity ($\frac{A}{Vm}$)
σ	Stefan-Boltzmann constant ($\frac{W}{m^2K^4}$)
τ	nominal residence time (s)
ψ	radial basis function
ω	chemical production rate of i-th species due to gas-phase reactions ($\frac{mol}{m^3s}$)
Γ	number of nanotube sites ($\frac{mol}{m^2}$)
Θ	approximate function
Θ_{BC}	boundary condition value
Φ	erosion rate ($\frac{kg}{s}$)
Ψ	basis matrix

1 Introduction

The discovery of C_{60} molecule in 1985 [5], multi-walled carbon nanotubes in 1991 [6] and single-walled carbon nanotubes in 1993 [7],[8] has greatly expanded the number of known carbon allotropes, which were until then limited to graphite, diamond, and amorphous carbon. The members of fullerene family exhibit remarkable strength and hardness as well as unique kinetic, electrical, optical and thermal features. Due to these novel properties, many suggestions for the application of these molecules have been made.

There is a number of different fullerene synthesis methods such as laser ablation technique, chemical vapour deposition, high pressure carbon monoxide and arc-discharge method. At present the most efficient production technique is the arc discharge method, discovered by Krätschmer [9], and its modifications [10], where fullerene yield reaches up to 20 %. The basis for these methods is arc discharge caused by electric current flowing through graphite electrodes in an inert gas atmosphere.

Since the fullerene formation is yet to be completely understood, several authors ([1], [2], [11]) have suggested various models. The review of some of these models is given in the paper as well the suggestion, which of the models is the most appropriate to be used for numerical simulations. All of the authors agree that the growth of fullerens can be described by four governing equations: continuity, energy, momentum and species conservation equation.

The governing equations of the suggested model will be solved numerically with a meshless method. This novel approach has several advantages over other standard numerical methods. The numerical solution is based on points instead of polygons, complicated can easily be calculated, non-uniform discretization represents no problem, etc.

In this method the solution is represented on the arbitrary set of nodes without any additional topological relations between them. The mesh-free method used in this case will be local radial basis function collocation method (LRBFC)[12].

2 Fullerenes

Fullerens are carbon forms that consist of spherical, cylindrical or ellipsoid arrangement of dozens of carbon atoms. Spherical fullerens are also called buckyballs, whereas cylindrical ones are called buckytubes or carbon nanotubes. The molecules from fullerene family have a range of unique properties as they are highly stable chemically and extremely strong, can be made to be magnetic, can be used as precursors for other materials, can resist extreme pressure, act as superconductors, absorb light and serve as lubricant.

2.1 Buckyballs

Spherical fullerenes or buckeyballs are formed of hexagon and pentagon units of carbon that are linked together to form a hollow geodesic dome with bonding strains equally distributed among the carbon atoms. The first fullerene molecule to be discovered was C_{60}, which is the smallest fullerene molecule in which no two pentagon units share an edge. C_{60} or Buckminsterfulleren, as it is commonly called, consists of 60 sp2 hybridized carbon atoms arranged as 20 hexagons and 12 pentagons. The van der Waals diameter of a C_{60} molecule is about 1 nanometer (nm), with nucleus to nucleus diameter of 71 nm and average bond length of 1.4 Å.

The family of fullerene molecules includes a variety of carbon clusters, from those as small as C_{20} to those as large as C_{240}. Apart from C_{60}, which is the most abundant, C_{70} and C_{84} are also commonly found. Example structures of the most common buckyballs are shown in the figures (1, 2 and 3 [15]) below.

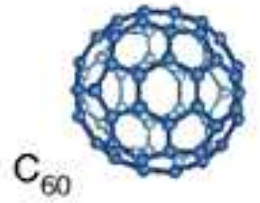

Figure 1: C_{60} [13]

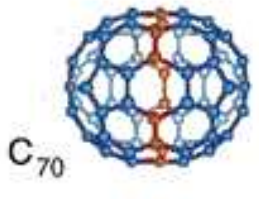

Figure 2: C_{70} [13]

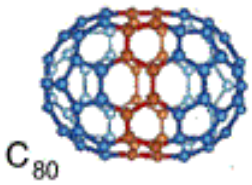

Figure 3: C_{80} [13]

2.2 Nanotubes

Cylindrical fullerenes or nanotubes are found in various forms: single-wall nanotubes (SWNT), double-wall nanotubes and multi-wall nanotubes (MWNT). Each of this forms can be produced selectively, depending on the growth process, which also influences length and diameter of a nanotube.

2.2.1 Single-Wall nanotubes

Graphene sheet is a single planar assembly of carbon atoms disposed in a honycomb lattice. The structure of the single-wall carbon nanotubes (SWNTs) consists of a graphene sheet rolled into a tube. If a nanotube is closed, such tube is capped by half a fullerene as depicted in a Figure 4. The structure of a nanotube can be conceptualized by taking this graphene

sheet and rolling it into a seamless cylinder. Different types of SWNTs are defined by their chirality, which indicates how the graphene sheet is wrapped. Chirality is described by chiral vector (m,n), where m and n are a pair of integers that denote the number of unit vectors along two directions in the honeycomb crystal lattice of graphene. Nanotubes are called "zigzag", if m=0, "armchair" if n=m and "chiral" otherwise (Figure 4). The diameter of a nanotube can be calculated from its (n,m) indices as follows [14]:

$$d = \frac{a}{\pi}\sqrt{(n^2 + nm + m^2)}, \tag{1}$$

where a = 0.246 nm. Most of the SWNTs have a diameter of about 1 nm and are several μm long. An example of SWNT bundles is represented in Figure 5, where SWNTs were observed through scanning electron microscope (SEM) and by transmission electron microscope (TEM).

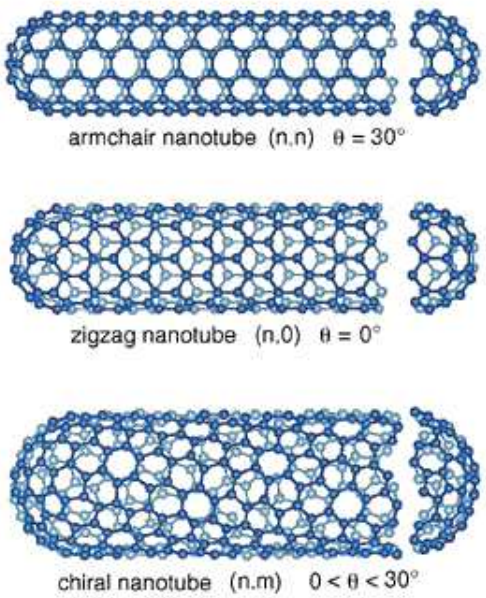

Figure 4: Examples of different types of single-wall carbon nanotubes sorted according to their chirality [15].

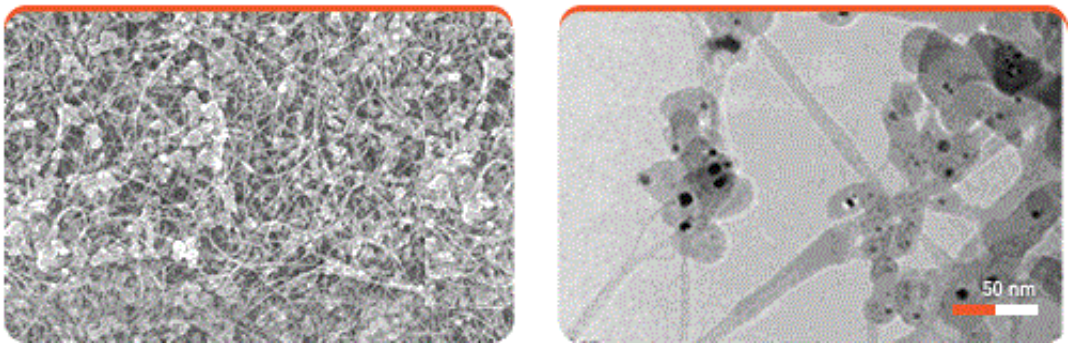

Figure 5: SEM (left) and TEM (right) images of SWNT bundles [16].

2.2.2 Multi-Walled nanotubes

Multi-walled nanotubes (MWNT) consist of multiple concentric layers of rolled graphene sheets. The structure of MWNTs is explained by two different models, both of which describe how the graphene sheets are rolled. In the Russian Doll model, sheets of graphite are arranged in concentric cylinders, which means that a SWNT is placed within a larger SWNT as depicted in Figure 6. In the Parchment model, a single sheet of graphene is rolled in around itself, resembling a scroll of parchment. The distance between walls in MWNTs is similar to the distance between graphene layers in graphite, which is approximately 3.4 Å. An example of MWNT bundles is represented in Figure 7, where MWNTs were observed under SEM and TEM microscopes.

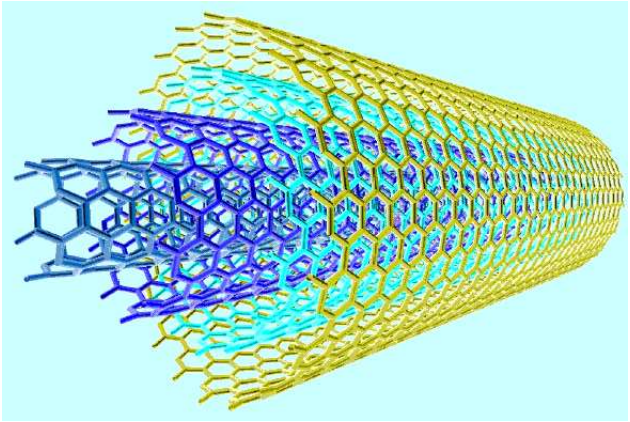

Figure 6: Multi-wall nanotube. [17]

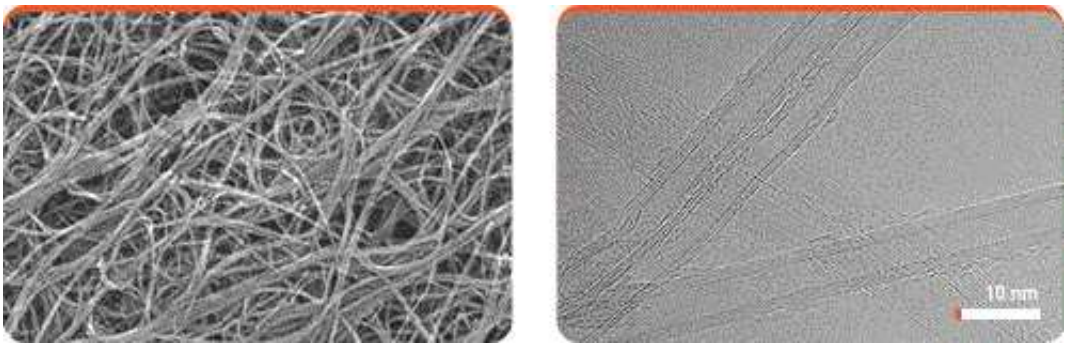

Figure 7: SEM (left) and TEM (right) images of MWNT bundles [16].

3 Fullerene production

This chapter was partialy written by Nataša Grlj [4].

The first method of production of fullerenes used laser vaporization of carbon in an inert atmosphere, but this produced microscopic amounts of fullerenes [5]. In 1990, a new type of apparatus using an arc to vaporize graphite was developed in Germany by Kratschmer and Huffmann [9]. Other commonly used technique for nanotube and fullerene production is chemical vapor deposition [20].

The carbon arc discharge method is the most common way to produce fullerenes and carbon nanotubes. However, it is a technique that produces a mixture of components and requires separation of desired product from the soot and the catalytic metals present in the crude product. This is also one of its major problems. In principle, this method creates fullerenes through arc- vaporisation of two carbon rods placed end to end, separated by a few millimeters, in an enclosure that is usually filled with inert gas (helium, argon) at low pressure (between 50 and 700 mbar). Recent investigations have shown that it is also possible to create nanotubes with the arc method in liquid nitrogen [21]. A current of 50 to 100 A driven by approximately 20 V creates a high temperature discharge between the two electrodes. The discharge vaporises one of the carbon rods and forms a small rod shaped deposit on the other rod and soot at the chamber walls. By controlling the parameters, one can control the yield and the types of the structures (fullerens, single-walled nanotubes (SWNTs), multi-walled nanotubes (MWNTs) etc.) produced. The method is explained in detail further on.

In the laser vaporisation method, a pulsed or continuous laser is used to vaporise a graphite target in an oven filled with helium or argon gas at some thousand degrees Celsius. A very hot vapour plume forms, then expands and cools rapidly. As the vaporised species cool, small carbon molecules and atoms quickly condense to form larger clusters, including fullerenes. For nanotubes, catalyst is used that also begin to condense, but more slowly at first, and

attach to carbon clusters and prevent their closing into cage structures. Catalysts may even open cage structures when they attach to them. From these initial clusters, tubular molecules grow into single-wall carbon nanotubes until the catalyst particles become too large, or until conditions have cooled sufficiently that carbon no longer can diffuse through or over the surface of the catalyst particles. It is also possible that the particles become that much coated with a carbon layer that they cannot absorb more and the nanotube stops growing. The fullerenes can also be produced by laser ablation of catalyst-filled graphite, but usually no catalysts are included in the target. However fullerene yields are not so high, since subsequent laser pulses excite fullerenes to emit C_2 that adsorbs on catalyst particles and feeds single-walled nanotube growth. Laser ablation in general is almost similar to arc discharge, since the optimum background gas and catalyst mix is the same as in the arc discharge process. This might be due to very similar reaction conditions needed, and the reactions probably occur with the same mechanism.

Chemical vapour deposition (CVD) synthesis is used mostly for producing nanotubes. It is achieved by putting a carbon source in the gas phase and using an energy source, such as a plasma or a resistively heated coil, to transfer energy to a gaseous carbon molecule. Commonly used gaseous carbon sources include methane, carbon monoxide and acetylene. The energy source is used to "crack" the molecule into reactive atomic carbon. Then, the carbon diffuses towards the substrate, which is heated and coated with a catalyst (usually a first row transition metal such as Ni, Fe or Co) where it will bind. Carbon nanotubes will be formed if the proper parameters are maintained. Excellent alignment, as well as positional control on nanometer scale, can be achieved by using CVD. Control over the diameter, as well as the growth rate of the nanotubes can also be maintained. The appropriate metal catalyst can preferentially grow single rather than multi-walled nanotubes. In the last decade, different techniques for the fullerene and carbon nanotubes synthesis with CVD have been developed, such as plasma enhanced CVD, thermal chemical CVD, alcohol catalytic CVD, vapor phase growth, aero gel-supported CVD and laser-assisted CVD.

Fullerenes are isolated from the soot created in the arc generator or in the reactor for laser vaporization usually by extraction with organic solvents [9, 22]. In general, toluene is used since it provides a sufficient solubility and is less toxic than benzene or carbon disulfide. Alternatively, hexane or heptane can also be used. The most common methods are a hot extraction of the soot followed by filtration and a Soxhlet extraction.

Soxlet extraction Soxlet extraction is a laboratory method, which is used to extract compounds from solid materials. It was originally designed for lipid extraction but is now used in a solvent in which a desired compound has limited solubility and the impurity is insoluble. A simple filtration or other separation technique can than be used in order to remove the desired component.Soxlet apparatus (Figure 8) consists of a glass reservoir, that

is situated between a flask containing the extraction solvent and condenser. The flask is heated after a solid material is palced into the glass reservoir. The material evaporates and moves up into the condenser where it converts into liquid. Liquid than drips back into the chamber containing solid material. When the chamber is full it overflows and is thus automatically emptied. The solvent and extract are siphoned back into the glass flask. The solvent reboils and the cycle is repeated until all of the desired component is extracted.

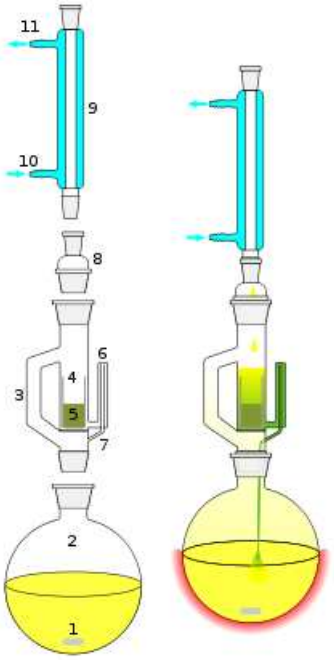

Figure 8: An example of schematic representation of a Soxhlet extractor [18].
1: Stirred bar.
2: Still pot.
3: Distillation path.
4: Thimble.
5: Solid.
6: Siphon top.
7: Siphon exit.
8: Expansion adapter.
9: Condenser.
10: Cooling water inlet.
11: Cooling water outlet.

The major issue of the fullerene/nanotube community is still the question of not how to produce fullerenes and nanotubes but how to make their production more economical, since this is still one of the most expensive material. The arc discharge method has proven the most promising for the commercial production of large quantities of fullerenes. However, the mechanism of the formation of fullerenes from carbon vapour is still not understood completely. In order to tune operational parameters to maximize the produced yield, one need to understand the processes in different parts of arc reactor. In this seminar, we present the state of the art in the field today.

4 Electric-arc discharge method

This chapter was partialy written by Nataša Grlj [4].

The carbon arc apparatus consists of a cooled (typically with water) reaction chamber with two cooled graphite rods (Figure 9). One is used for the anode that can be filled with catalysts (Co, Fe, Ni, Y), the other is cathode usually made of pure graphite. Sometimes copper is used, but it does not bring any advantage and leads to a more unstable arc. The distance between the anode and the cathode can be changed and controlled. A current passes through electrodes, direct for nanotube synthesis, alternating for fullerene production. Between electrodes, plasma is created. For efficient operation, the plasma must be stable and the anode erosion rate constant. This can be achieved by maintaining a constant voltage between the electrodes – ergo by keeping an eye on the space between the electrodes. At the beginning of the process, the rods are in contact and the electric current elevates the temperature of the contact point until the anode material starts to evaporate and the plasma is ignited. Then, the anode is moved back to maintain the desired gap between the burning anode and the cathode. Deposit starts to grow on the cathode side. Plasma is bounded by the deposit and the anode and consists of carbon and catalyst vapour, which diffuse to the cooled reactor regions. The high temperature near the anode and the high energy density in the plasma ensure the vaporisation of most of the anode material. Since the cathode is water-cooled, the plasma quench at the edges and a high rate of supercooled and supersaturated vapor ensures nanotube or fullerene formation. The arc products are soot on the reactor walls, web-like structures between the cathode and the chamber walls, deposit at the end of the cathode and a collaret around this deposit.

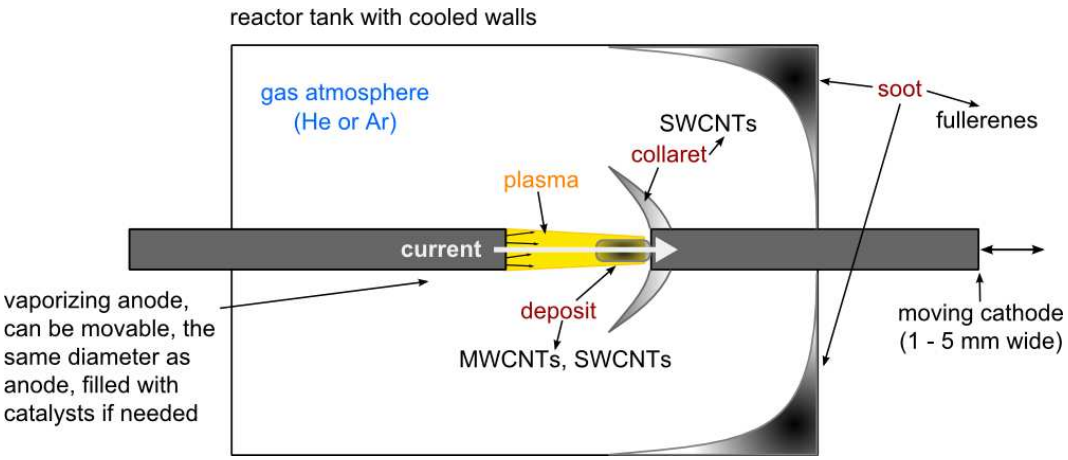

Figure 9: The scheme of a typical arc discharge reactor chamber and the locations where products are formed [4].

Fullerenes are created outside of the inter electrode gap and can be found in the soot around the reactor walls, the columnar structure of the cathode deposit is rich with multi-walled carbon nanotubes (MWCNTs), while single-walled nanotubes (SWCNTs) can be found in the collaret. Several parameters are responsible for successful fullerene production, such as pressure of the buffer gas, its type, temperature of plasma, the current applied on the electrodes and the distance between them in order to maintain a stable arc. This governs energy transfer, dissipation and loss that are responsible for the amount of fullerene produced. This is the topic of the next sections.

5 Fullerene synthesis

5.1 Experimental

This chapter was partialy written by Nataša Grlj [4].

First attempts to understand the connection between mentioned parameters and to increase fullerene yield were experimental. Saito et al. [23] reported that the fullerene yield was a function of the inert gas type and pressure and maximum yield of 13 wt% was obtained at the helium pressure of 2.6 kPa and DC current in the range of 220-250 A. C_{70} and higher fullerenes showed maximum abundance at slightly higher pressure, up to 6.6 kPa. Argon did not appear as promissing gas [23]. The attempt of Weston and Murthy to optimize process parameters of arc method lead to yields up to 6% [24]. Huczko et al. reported the value of 20% for fullerene yield at 13.3 kPa for pressure of helium and the 65 A of DC current [25]. The same group also studied the electrode gap dependence to the fullerene yield [26]. The maximum of 15 wt% was obtained for small distances (less than 1 mm), at 13.3 kPa of He gas and a current of few tenths of A. The yield decreased with the increasing distance. Marković et al. studied pressure and current dependence of fullerene yield as well [27]. The local maximum was found to be at the helium pressure of 8 kPa and the current of 60-70 A. Yield in this conditions reached 8%. They also made some attempts to theoretically understand the obtained results. Krestinin and Moravsky obtained 20 - 25% fullerene yield at pressure of around 13 kPa and the arc current of 60-70 A [28]. They argued that this yield is the limit attainable in electric-arc synthesis [29]. Sugai et al. produced fullerenes and carbon nanotubes by high-temperature pulsed arc discharge [30]. They reached 7.9 wt% of C_{60} yield for 3 ms long pulses at high temperature around 1000°C. For longer pulses the yield decreases. Surprisingly, they found Kr and Ar to be much more effective as the buffer gas than He. The group of Marković later also studied temperature dependence of arc plasma on the yield [31]. Dubrovsky et al. applied buffer gas outflow in the standard arc generator in order to reduce the cathode deposit and increased fullerene yield. They obtained 8% at DC current near 1100 A but increased fullerene productivity up to 60 g/h and reduced production costs [32].

Song et al. studied the effect of furnance temperature on fullerene yield by the first time [33]. They found strong temperature dependence. At 10 kPa of He and 90 A current, the obtained fullerene yield was only 5.3 % at room temperature, however it increased to 30.6 % when the temperature was set at 200°C. By further increasing the temperature, the yield decreased.

An extensive experimental characteristics in the arc zone were investigated by Saidane et al. [34]. Here, the authors aim was to provide better understanding of the effects of macroscopic discharge parameters on the local plasma properties and the resulting fullerene yield. The concentrations of the C_2 radicals (fullerene precursors – look next subchapter) and the temperature fields were mapped in the arc plasma under various arcing conditions (gas pressure, arc current and the anode sublimation rate). These parameters were compared to the C_{60} yield in the produced soot. Some results are shown in Figure 10. Again, the best yield obtained at 13 kPa, 75 A and the inter-electrode distance of 1 mm was 12 %. They also stated an important parameter is the base pressure - the pressure at which the arc chamber is typically evacuated before injecting the helium. It should be in the order of 10^{-1} Pa and should be kept under 10 Pa by any means.

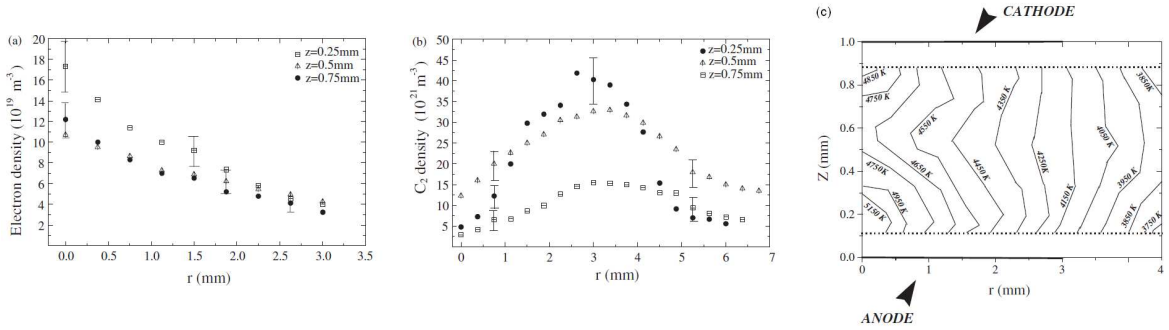

Figure 10: Radial electron density profiles (a), radial profiles of the density of the C_2 molecule (b) and the measured map of the temperature field in the area between the electrodes (c). Measurements were performed at $I = 65$ A, $P = 13$ kPa and the distance between electrodes was 1 mm. Results are taken from [34].

In the amount of experimental data (normally, the presented articles do not cover all the experiments performed up to now) we can derive some conclusions. The fullerenes can be found in the soot. The major type of fullerenes produced is C_{60} followed by C_{70}, the bigger molecules are produced only in traces. The ratio C_{70}/C_{60} is almost constant and around 0.2. The optimal current is several tenths of amperes, while the optimal pressure of helium (that has mostly proven to be better choice) is around 13.3 kPa (100 Torr). The yields are usually around 10%, up to 20% was obtained, however 20-25% is supposed to be the limit. In the

part that follows, some explanation of these facts is given.

5.2 Fullerene growth - mechanisms

This chapter was partialy written by Nataša Grlj [4].

There is still no common theory describing the mechanism of fullerene formation and destruction. In the arc, carbon ions and electrons are the material that forms the majority of the plasma. Carbon is removed from the arc gap by a gas-plasma jet. In the jet, the carbon atoms condense into clusters as the gas cools. C^{12}/C^{13} isotopes scrambling experiments demonstrated that the first stages of fullerene formation require the presence of small carbon clusters as a precursor [35, 36]. There are two major theories that describes the formation of larger closed structures from graphite evaporation – the "pentagon road" and the "fullerene road" (see [37] and references within).

5.2.1 The pentagon road

Isolated pentagon rule, or pentagon road, was among the first proposed theories that managed to explain observed properties. The pentagon rule assumes that fullerens are formed from energetically the most favoured form of an open graphene sheet. In order to insure this criteria the following conditions known as the pentagon rule must be true: graphene sheet is made up solely by pentagons and hexagons, it has as many pentagons as possible and it avoids adjacent pentagon units. Graphene sheets are formed for cluster with more than 30 C atoms. Smaller carbon configurations are than ingested into the graphene sheet. Since it is assumed that the process must follow the low energy path, pentagonal units are incorporated between the hexagonal ones. With the addition of pentagon units the sheet curls up and thus reduces the number of dangling bonds. Sites where two pentagons share a bond are avoided due to the curvature introduced by the bond, whose hybridisation changes from sp^2 to sp^3. The C_{60} is the first pentagon rule structure that is closed.

5.2.2 The fullerene road

The Fullerene Road suggests that fullerens form from clusters with more than 40 atoms and grow either by the addition of smaller carbon clusters or by opening and reclosing until they reach C_{60}. Odd clusters when formed are very reactive, which is why they are easily converted to fullerenes by loss or extraction of a C atom. The adjacent pentagon bonds are removed by ring rearrangement.

A growth mechanism for Fullerene Road scheme is similar to the Pentagon Road (addition of small carbon fragments), but the intermediate all-carbon molecules with 30-58 atoms are, like the larger products, closed fullerene cages. Because these small fullerenes cannot obey

the isolated pentagon rule, they are more reactive than the larger ones, with the 5-5 ring junctures serving as activated sites for addition of C_2. Thus, C_{60} and C_{70}, if formed as the isolated pentagon isomers, act as end points of cluster growth. As with the Pentagon Road mechanism, the Fullerene Road as stated, requires a large concentration of C_2 and C_3, even at the later stages of cluster growth. The comparison of the Fullerene Road mechanism with the Penatagon Road mechanism with stable fullerene isomers is depicted on Figure 11.

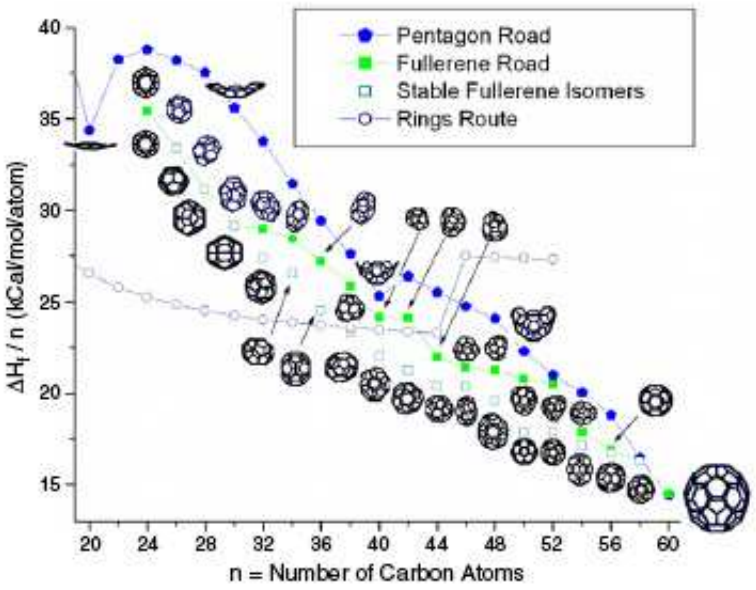

Figure 11: Comparison of different fullerene growth models [19]. Growth of C_{60} from C_{24} is modeled for both fullerene and pentagon road. Additionally, the growth of C_{60} via Rings route is presented for comparison. In Rings Route model carbon rings fuse together to form closed fullerene shells. The best agreement to stable fullerene isomers is achieved with fullerene road model.

6 Purification

In order to acquire a significant amount of nano material from a mixture of components produced in the arc-discharge synthesis, material has to be purified. Purification techniques such as funcionalisation (in diethylether or GPC), filtration, cross flow filtration or ultrasonication in alcohol can be effectively used to separate fullerenes as well as nanotubes, carbon particles and metal catalysts, while others e.g. thermal oxidation (for metal catalysts), high temperature vacuum treatment (for SWNT) and magnetic purification (for SWNT, C_{60} and carbon particles) can only be used for separation of some of the products. Different techniques are

used to achieve different results. As the selected technique affects an entire sample, care has to be taken in choosing the appropriate technique.

Fullerene: Purification techniques used for fullerene C_{60} and C_{70} separation are: HNO_3 treatment, mild acid treatment, functionalisation (in diethylether), funcionalisation (HPC), magnetic purification, HPLC (size separation), sonication (in alcohol), ultrasonication (in acid), cutting through flourization, filtration and cross flow filtrations.

Nanotubes: Purification techniques used for SWNT extraction are: HNO_3 treatment, mild acid treatment, functionalisation (in diethylether), funcionalisation (HPC), magnetic purification, vacuum annealing, high temperature annealing, high temperature vacuum treatment, HPLC (size separation), sonification (in alcohol), filtration, cross flow filtrations and CS_2 filtration.

7 Models of fullerene growth

Fullerene production has been studied extensively ([1], [2], [28], [38], etc.) in order to optimize the parameters necessary to increase fullerene yield. The process of fullerene formation is very complex with many variables involved. Although, the complete picture of its kinematics is still unknown, many models exist that are in satisfactory agreement with experiments.

In order to describe the fullerene synthesis mathematically, the fields of velocity, temperatures, carbon mass fraction and current intensity in the arc reactor must be determined. It is believed by the majority of authors [2] that as a consequence of mass and heat transfer due to the electrode evaporation, a fan jet is formed.

A short overview of fullerene modeling is given in the next chapter.

7.1 Models of the fullerene growth -review

This chapter was partialy written by Nataša Grlj [4].

From the beginning of fullerene production, there have been attempts to describe mathematically the situation in the arc and around in order to optimize the parameters necessary to increase the fullerene yield. The task turned out to be rather difficult, since there are many variables involved and the precise kinematics of fullerene production is still not known. Therefore, the complete picture is not built yet, however many models exists that give satisfactory agreement with the experiments. Here, we present the model of Krestinin and Moravsky [28, 29], of the group of Bilodeau [1], of Marković [38] and the work of Aleksejev and Dyuzhev [40, 41, 42, 3, 43].

In order to describe the processes of fullerene synthesis mathematically, it is necessary to determine the velocity and the temperature distribution around the arc in the atmosphere of the inert gas. Knowing these distributions, one can calculate residence time of the carbon clusters in different zones. Several authors claim that as a result of the electrode evaporation and mass and heat transfer process, a fan jet is formed [28, 38, 43]. Therefore, the kinetic model of the fullerene formation process in the jet have to be made. This is the path followed by the majority of authors.

7.1.1 One-dimensional model

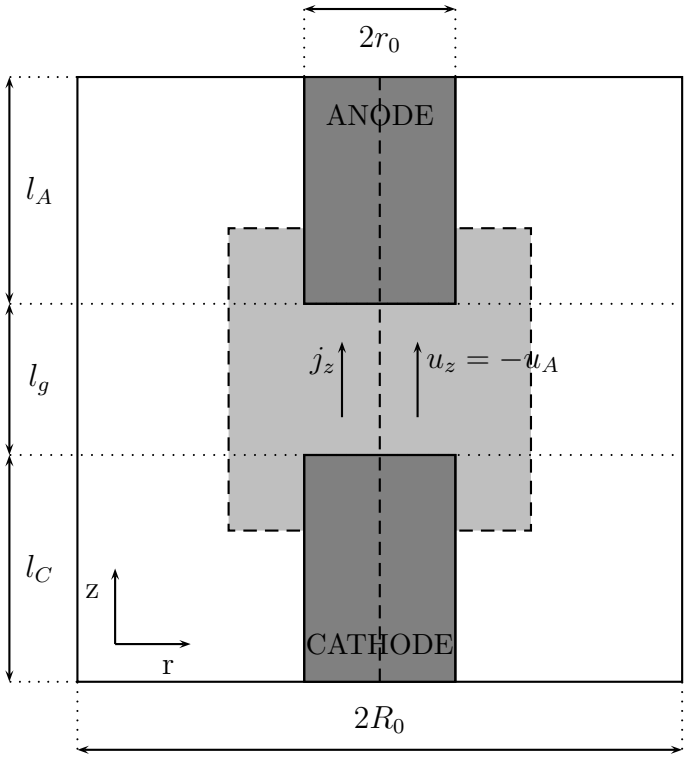

Figure 12: Model domain representation. Here marks anode length, marks gap distance, marks cathode length, marks axial velocity, marks anode gas velocity, marks axial current density, 2 marks anode and cathode diameter and 2 marks the reactor chamber diameter.

Farhat et al. [2] developed a one-dimensional model (Figure 12) that solves for species, temperature, and velocity profiles in a steady state stagnation point flow and incorporates temperature dependent properties. The model is formulated for nanotube growth in the

inter-electrode region. It is a boundary value problem that consists of a set of differential equations and is solved by the finite differences method. Local thermal equilibrium (LTE) is assumed based on the model of Bilodeau et al. [1] as well as a steady state, which is justified by continuous adjustment of electrodes, which assures a constant erosion rate at the anode and consequently a constant condensation of carbon vapor near the cathode. Gas-phase chemical reaction mechanism is added into numerical simulations to represent the carbon condensation. In the model carbon deposition on the cathode is accounted for by a set of surface reactions that describe nanotube growth. A set of governing equations include continuity equation:

$$\frac{\partial \rho}{\partial t} = -\frac{u_z}{\rho}\frac{\partial \rho}{\partial z} - 2V - \frac{\partial u_z}{\partial z} = 0 \tag{2}$$

radial momentum equation:

$$\rho\frac{\partial V}{\partial t} = -\frac{\partial}{\partial z}\left(\mu\frac{\partial V}{\partial z}\right) - \rho u_z\frac{\partial V}{\partial z} - \rho V^2 - \frac{1}{r}\frac{\partial P}{\partial r} = 0 \tag{3}$$

species conservation equation:

$$\rho\frac{\partial Y_i}{\partial t} + \frac{\partial(\rho Y_i V_i)}{\partial z} + \rho u\frac{\partial Y_i}{\partial z} = M_i\omega_i \tag{4}$$

and energy equation:

$$\rho c_p\frac{\partial T}{\partial t} = \frac{\partial}{\partial z}\left(k\frac{\partial T}{\partial z}\right) - \rho c_p u_r\frac{\partial T}{\partial z} - \sum_{i=1}^{n_g}\left(c_{p_i}\rho Y_i V_i\frac{\partial T}{\partial r} + \omega_i h_i\right) + S_q - Q_{rad} = 0 \tag{5}$$

The solutions for these equations are obtained for their steady state form. In these equation is a distance normal to the cathode, is time, is axial velocity, is radial rescaled velocity, is temperature, is gas-phase species mass fraction, is mass density, is specific heat at constant pressure, is the molecular weight, is a specific enthalpy, is thermal conductivity, is viscosity, is the net chemical production rate by gas-phase reaction, is diffusion velocity, is the energy source term and is the net loss of energy by the radiation. Index denounces different species.

SPIN [48], CHEMKIN [51] and IVTANTHERMO [52] program codes and databases were used to solve the full chemical reactions model.

7.1.2 Two-dimensional models

Krestinin and Moravsky developed a mathematical model 13 for the fullerene synthesis in the arc reactor [28] and combined it with the kinetics of fullerene formation [29]. The model considers the outflow of the carbon vapour from the electric arc interelectrode gap, its blending

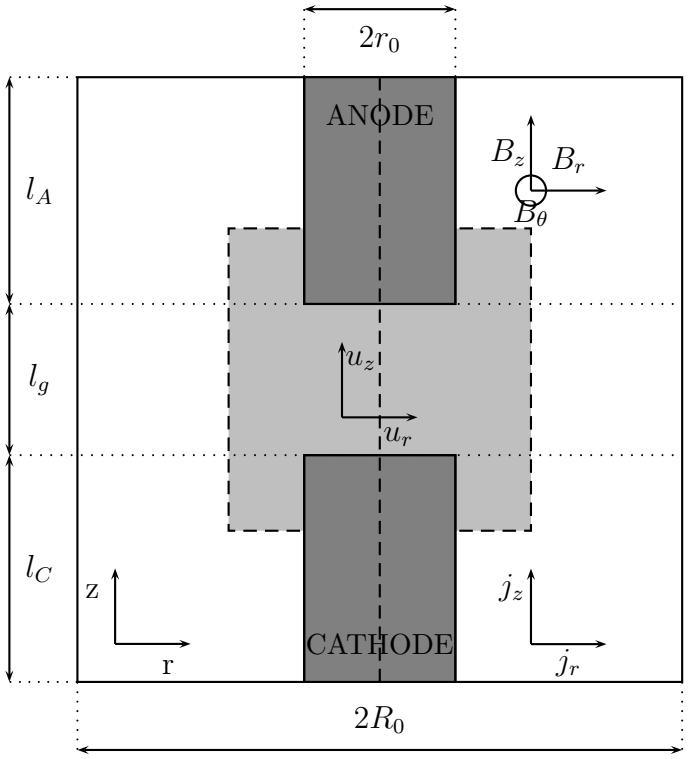

Figure 13: Model domain representation. Here l_A marks anode length, l_g marks gap distance, l_C marks cathode length, u_z marks axial velocity, u_A marks anode gas velocity, u_r marks radial velocity, j_z marks axial current density, j_r marks radial current density, $2r_0$ marks anode and cathode diameter and $2R_0$ marks the reactor chamber diameter.

with helium gas and cooling, the kinetics of the reactions of carbon vapour condensation, and the formation of soot particles and heterogeneous reactions at their surface. To describe the carbon vapour condensation, the parameters of the gas issuing from the arc zone into an inert atmosphere should be known. The authors argued that no quantitative theory of an arc with electrode evaporation had been developed at that time, therefore exact calculation of this parameters was not performed. The authors calculated the fullerene yield and C_{60}/C_{70} ratio, which was found to be constant in the experiments, in dependence of the buffer gas pressure and electric current. Several assumptions were made and the authors confined themselves only to those experiments in which the following conditions can be met: a) the stream of carbon vapour from the arc region forms a turbulent flow that can be idealized as a so-called fan flow – a flat flow of cylindrical geometry, b) the rate of the inert gas diffusion inward the inter-electrode zone is much less than the mass flow of carbon vapour from the gap (this

condition is fulfilled when the arc gap is small enough), and c) the temperature gradient in the gap between the electrodes can be neglected (this assumption should be taken with great care, as we will see further on in other models).

In this way, the gas leaving the arc can be treated as pure carbon vapour and with the assumption that it is equilibrated with the temperature of the electrode graphite, the velocity of the stream v_0 can be calculated as:

$$v_0 = \frac{V_{\mathrm{SOOT}} R T_0}{2\pi r_0 h_0 P}, \tag{6}$$

where V_{SOOT} is the rate of fullerene soot formation obtained experimentally, p is helium pressure in the reactor, R is the gas constant, r_0 is the radius of electric rods, h_0 is the arc gap, T_0 is vapor temperature, that the authors establish to stem from the equation $p_{eq}(T_o) = P$, where p_{eq} is the equilibrium pressure of the carbon vapor. They also assumed that the temperature T_0 lies in the range of 3600 - 3900 K and the pressure of helium in the reactor is is between 13.3 and 93.3 kPa.

In the model, the equations governing the flow within a boundary layer with turbulent mass and heat transfer across the jet are obtained from the continuity and Navier-Stokes equations and are as follows (7):

$$\begin{aligned} \rho v \frac{\partial a_i}{\partial r} &= \frac{\partial}{\partial z} \kappa_c \epsilon_\tau \rho \frac{\partial a_i}{\partial z} + M_i f_i; \quad i = 1, \ldots, N \\ \rho c_p v \frac{\partial T}{\partial r} &= \frac{\partial}{\partial z} \kappa_T \epsilon_\tau \rho c_p \frac{\partial T}{\partial z} + f_T \end{aligned} \tag{7}$$

In the upper equation, ϵ_τ is the coefficient of the turbulent momentum transfer, κ_T and κ_c are the empirical coefficients relating momentum transfer to mass and heat transfer, a_i is the relative mass fraction of the species i, T is the temperature at the radial position, f_i and f_T are the rates of mixture component formation and the rate of heat release due to chemical reactions per unit volume, M_i are the molecular weights of the mixture components, ρ is the gas density, c_p the mixture specific heat and v the mean gas velocity.

To solve these equations, the semi empirical theory of free turbulent jet [39] was applied. In this theory, the half-width of the turbulent jet, b(r), is related to the mixing length L by a linear equation $L/b = \text{const.} \approx 0.2$. Near the jet center, derivatives of all the functions with respect to z equal zero because of the jet symmetry. Therefore, the temperature and concentration values vary only little within the mixing length L(r) and are assumed constant and equal to their values in the $z = 0$ plane. Therefore, the equations 7 are first integrated with respect to z over interval $[-L, L]$, in the result the derivatives are replaced by finite differences and all the previously stated assumptions are taken into account. The detailed

description of the calculation procedure is described in the article. As a result, authors obtained the set of ordinary differential equations for approximate description of an elementary gas volume moving near the symmetry plane of the fan jet (8).

$$\begin{aligned} \frac{d\alpha_i}{dt} &= k_c(\alpha_{0,i} - \alpha_i) + \frac{f_i}{[M]}, \quad i = 1, 2, \ldots, N \\ \sum_{i=1}^{N} \alpha_i c_{p,i} \frac{dT}{dt} &= \sum_{i=1}^{N} \alpha_i c_{p,i} k_T (T_{at} - T) + \frac{f_i}{M}, \end{aligned} \tag{8}$$

where α_i and $\alpha_{0,i}$ are mass fractions of mixture components in the reactor volume and buffer gas, M is the mole gas concentration, $c_{p,i}$ is the specific heat capacity at constant pressure of the i-th species. For the mass and heat transfer coefficients k_c and k_T the authors obtained empirical Formulas 9 and 10:

$$k_c = \frac{0.32}{\tau_{mix} + 2t}, \tag{9}$$

$$k_T = \frac{0.64}{\tau_{mix} + 2t}. \tag{10}$$

τ_{mix} is the representative time of turbulent mixing calculated from the flow velocity in the jet within the arc zone v_0 . It depends on the initial experimental parameters

$$\tau_{mix} = \frac{r_0}{v_0}\sqrt{\frac{r_0}{h_0}}. \tag{11}$$

In the suggested model, τ_{mix} is the parameter that specifies the rate of cooling and mixing and the fullerene yield in the product should depend on this value. Experimental data shown in Figure 14 confirms that. For explicit calculation of the fullerene yield, the kinematics has to be developed as well, and the final results of the model are also represented in Figure 14 (right graph).

In their article from 1998, Bilodeau, Pousse and Gleizes [1] described a two-dimensional model for the analysis of the carbon arc reactor for fullerene synthesis. The momentum, energy and carbon conservation equations were solved. The model accounts for carbon evaporation from the anode, deposition on the cathode and condensation in the regions surrounding the arc. Erosion rates were determined experimentally in a typical carbon arc reactor consisting of two opposed, movable graphite electrode rods separated by a distance of one to a few millimeters and housed in a vacuum vessel for this purpose. A pressure of 13.3 kPa of helium and a current of 80 A were used. Fields of the velocities, temperatures, and mass fraction of carbon in the gas are presented for 1 and 4 mm arcs in helium (some results

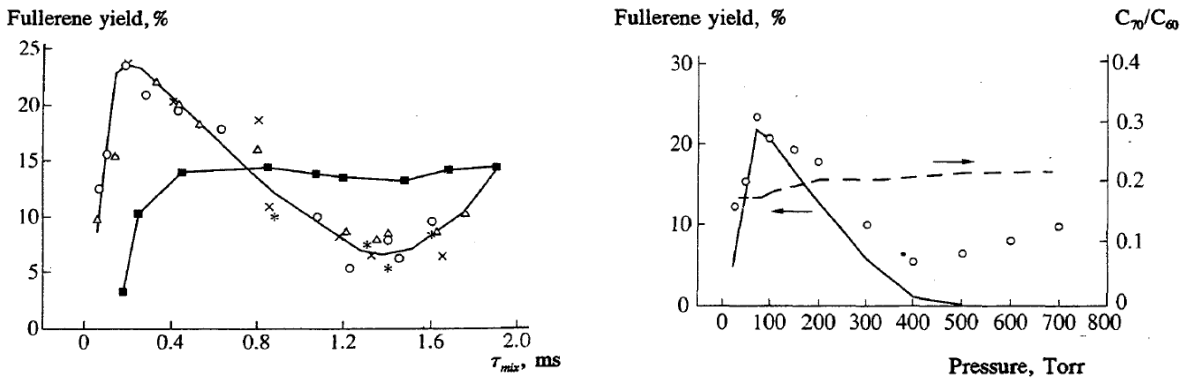

Figure 14: Left: Experimental data on the fullerene yield represented as dependent on the characteristic time of turbulent cooling and mixing. The common solid line represents the dependence. The experimental points corresponding to the current of 100 A (■) show that in this case the turbulent transfer does not control the process of mixing. The △ represents data acquired at the 55 A , × at 60 A and ∗ at 70 A arc current. Right: The helium pressure dependence of the fullerene yield (solid line, dots) and the molar ratio (dashed line) in the products of arc synthesis. Presented is the comparison between experimental (circles) and calculated data (solid line). The experiments were run at an arc current of 65 A. The results are taken from [28].

are presented in Figures 15 and 16). Comparisons were made between helium and argon as buffer gases, at 4 mm gap length. The authors assumed the temperature range between 2000 and 3000 K to be favorable for the formation of fullerene precursors ([1] and references in the article), and for that range, higher carbon species concentrations were calculated in helium than in argon.

Several assumptions were made in the model. The authors assumed axisymmetric laminar flow, steady state (the electrodes are continuously adjusted in order to maintain a constant interelectrode gap), local thermodynamic equilibrium, constant uniform anode erosion rate, a one-dimensional electric field, the assumption that the deposition on the surface of the cathode is supposed to be governed by diffusion only (the drift velocities of ions due to electric field are one order of magnitude lower than the bulk velocities in plasma and can be neglected) and the input of energy in the arc is due to ohmic heating and due to the enthalpy flux of the electrons only.

Authors solved continuity equation (12), the equation for the conservation of momentum (13), of energy (14) and of carbon species (15):

$$\vec{\nabla} \cdot (\rho \vec{v}) = S_m \tag{12}$$

$$\vec{\nabla} \cdot (\rho \vec{v} \vec{v}) = -\vec{\nabla} p + \vec{\nabla}(\mu \vec{\nabla} \vec{v}) + \rho \vec{g} + \vec{j} \times \vec{B} \tag{13}$$

$$\begin{aligned} \vec{\nabla} \cdot (\rho \vec{v} h) &= \vec{\nabla} \cdot \left(\frac{\kappa}{c_p} \vec{\nabla} h \right) + \frac{j_z^2}{\sigma} + \frac{5}{2} \frac{k_B}{e\, c_p} \vec{j} \cdot \vec{\nabla} h - \\ &- \vec{\nabla} \cdot \left(\frac{\kappa}{c_p} - \rho D_c \right) (h_c - h_g) \cdot \vec{\nabla} \omega_c - 4\pi \epsilon_n + S_h \end{aligned} \tag{14}$$

$$\vec{\nabla} \cdot (\rho \vec{v} \omega_c) = \vec{\nabla} \cdot (\rho D_c \vec{\nabla} \omega_c) + S_m \tag{15}$$

In these equations, $\vec{v}$ is the gas velocity, p is the local pressure, μ is the viscosity, ρ the mass density, g the gravitational acceleration, h is the specific enthalpy, while h_c and h_g are the enthalpy of pure carbon and pure buffer gas, κ is the thermal conductivity, c_p the heat capacity at constant pressure, ϵ_n is the net emission coefficient, e the charge of the electron, k_B is the Boltzmann constant, σ the electrical conductivity, ω_c is the mass fraction of carbon species and D_c the diffusion coefficient of the carbon species. S_m is the mass source term. It can represent the carbon evaporation near the anode, where its value is fixed experimentally. On the cathode face it represents carbon deposition by diffusion. Where supersaturation is reached in the gas phase, S_m constitutes a negative source term due to condensation and is expressed in the form of a nucleation rate. S_h is the enthalpy source term corresponding to S_m. The axial current intensity $j_z = \sigma E$ is calculated from the linear electric field E, the conductance Z, the total current intensity I and the radius of the electrodes: $E = I/G$, $G = 2\pi \int_0^R \sigma r dr$.

The group of Marković [38] followed similar path. They showed that the formations of so-called magic fullerenes (C_{60} and C_{70}) had two phases: the formation of liquid carbon clusters and their crystallization in the investigated fullerenes by the emission of atoms and small clusters. All phases of the formation (the formation of chains, rings, defective fullerenes and annealing) are strongly effected by the residence time τ in corresponding temperature region. τ is related to the temperature gradient and jet velocity (20). Fullerene synthesis therefore requires certain time in order to complete, and the residence time determines the value of the yield. They deduced that the maximum possible yield of C_{60} is 20 %.

In order to obtained temperature distribution of graphite arc, the authors solved Elenbaas-Heler equation:

$$\frac{1}{r} \frac{d}{dr} \left(r k(t) \frac{dT}{dr} \right) + \sigma(T) E^2 = 0 \tag{16}$$

that is in basis the energy conservation equation. In the cylindrical coordinate system can be written in the form (17):

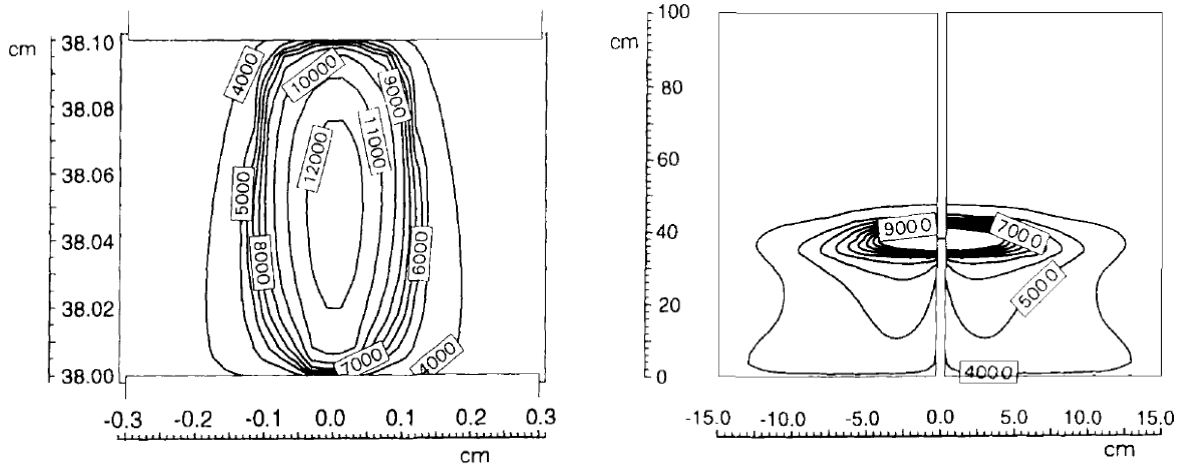

Figure 15: Temperature in the interelectrode gap (left) and temperature field in the whole reactor (right). The maps were obtained for helium buffer gas with pressure 13.3 kPa, current of 80 A and interelectrode distance 1 mm. The results are taken from [1].

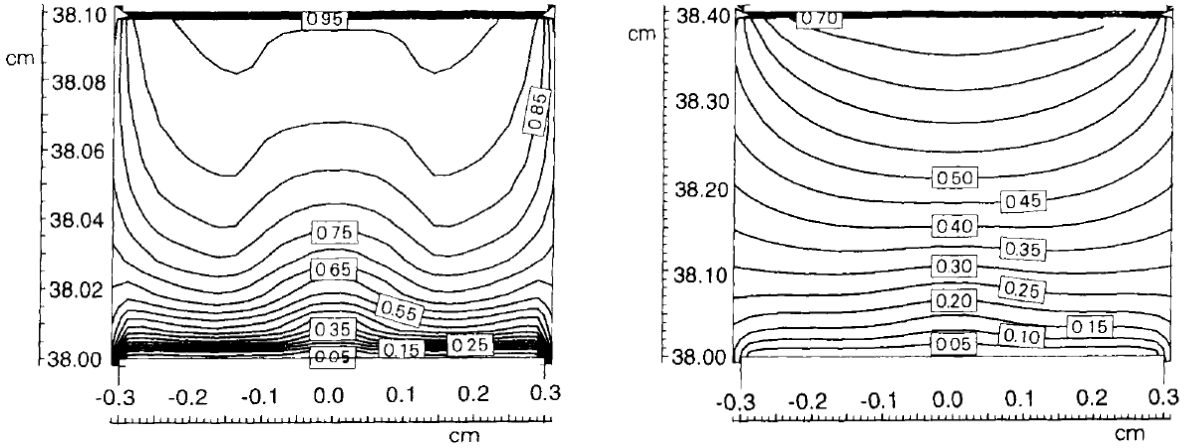

Figure 16: Carbon mass fraction in the interelectrode gap for 1 mm gap (left) and 4 mm gap (right). The maps were obtained for helium buffer gas with pressure 13.3 kPa and current of 80 A. The results are taken from [1].

$$c_3 E_z^2 p^{-\frac{1}{2}} T^{\frac{3}{4}} e^{-\frac{e_O u_i}{2kT}} = \frac{d}{dr}\left(r\chi(T)\frac{dT}{dr}\right) + c_4 \frac{p}{T} e^{-\frac{e_O u}{kT}} \tag{17}$$

c_3 and c_4 are constants and are calculated on the basis of values of the total power of the carbon arc and the radiation power. E_z is the interelectrode electric field, p the pressure of the buffer gas, u_i the ionization potential, u the effective excitation potential, $\chi(T)$ the heat conductivity that has a linear temperature dependence up to 12000 K, T the gas temperature and r the distance from the arc axis.

For the mathematical description of the fullerene formation the authors used the kinetic model based on the work of Neruev (see [38] and the references within). There the system of differential equations (18) describes the change in the concentration c_n of a cluster C_n, due to the formation from smaller clusters and due to the consumption of the cluster C_n in the process of formation of bigger clusters.

$$\frac{dc_n}{dr} = \frac{N_c}{v}\left(\sum_{j=1}^{n} K_{n-j,j}c_{n-j}c_j - \sum_{j=1}^{\infty} K_{nj}c_n c_j - K_{nn}c_n^2\right), \tag{18}$$

where N_c is the carbon concentration in the inter-electrode space and v is the helium jet velocity that transport carbon clusters. Value of K_{ij} are reaction constants between clusters C_i and C_j and are given by:

$$K_{ij} = \sqrt{\frac{i+j}{i\cdot j}}\sqrt{\frac{8k_BT}{\pi M_c}}\sigma_{ij}Ke^{-\frac{E_a^{ij}}{k_BT}}. \tag{19}$$

In the above equation, T is the reaction temperature, M_c is the mass of the carbon atom, σ_{ij} is the corresponding cross section, $p_{ij} = e^{-\frac{E_a^{ij}}{k_BT}}$ describes the probability of the reaction, E_a^{ij} is the activation energy for the appearance of the cluster C_{i+j} and K is the collision factor.

On the basis of the numerical analysis combined with some experimental facts, temperature distribution of the contact can be determined. For the arc axis temperature 6000 K, the current of 80 A, the helium gas pressure 13.3 kPa and the distance between electrodes 5 mm, the result is presented in Figure 17. The residence time of the carbon clusters in the temperature region from 6000 to 2400 K (the lowest temperature, where the annealing of the fullerenes take place) can be described as:

$$\tau = \int_{r(6000\text{K})}^{r(2400\text{K})} \frac{dr}{v(r)} = \frac{1}{\kappa V_g\sqrt{8.3}d}\int_{r(6000\text{K})}^{r(2400\text{K})} r dr, \tag{20}$$

where V_g is the maximum gas velocity and κ presents the relation between actual and maximum jet velocity.

Several interesting results followed, one is the explanation why is helium better choice for the buffer gas than argon. The axis temperature in a helium atmosphere can be raised

much higher than in argon and this influences the residence time in the high temperature zone. Heat conductivity of argon is two orders of magnitude smaller than the conductivity of helium, which leads to higher decrease of temperature in the neighborhood of the arc. Therefore, fullerene growth in argon starts at lower temperature and lasts less time than in helium. The result of the calculation of the fullerene yield is presented in figure 18.

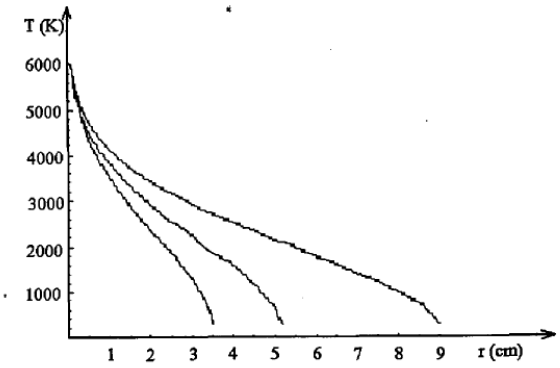

Figure 17: The temperature distribution of arc burning in helium with axis temperature $T_0(r = 0) = 6000$ K. The results are taken from [38].

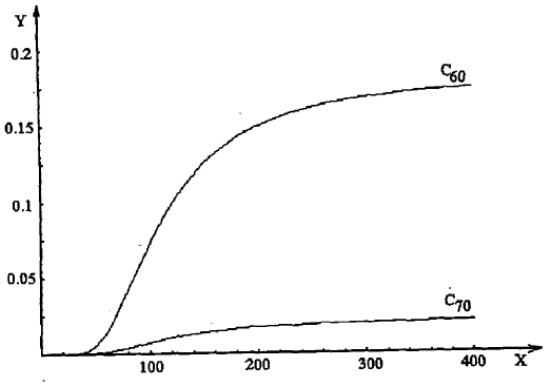

Figure 18: Yield of fullerenes C_{60} and C_{70} as a function of variable X. $X = r\frac{N_c\sigma_{ij}}{v}\sqrt{\frac{8k_B}{\pi M_c}T_0}p_{ij}$. The results are taken from [38].

In addition to, Aleksejev and Dyuzhev published a series of articles [**?**] regarding the formation of fullerenes with arc method. Their work addresses variety of aspects in the process; first the kinetics of fullerene growth and the quantum-chemistry calculation of this

mechanism was performed [40, 42], the transformation of carbon vapour in the gas-plasma jet was described [42, 3], and the results were used in the model of electron arc and the jet in order to find the connection between initial jet parameters and the fullerene yield [43]. Partial overview of the results were written in [44]. Nice presentation of the fullerene formation is schematically presented in Figure 19. The stages of fullerene formation are as follows. In the arc, the plasma consist of the material evaporated from the electrode atomic (ionized) carbon, some small (ionized) carbon molecules, gas atoms and electrons. Carbon is removed from the arc by a gas-plasma jet. Initial characteristics of the jet (carbon concentration, gas temperature and the initial velocity of the jet) are obtained from calculations of the fullerene arc discharge. In the jet, the carbon atoms condense into clusters as the gas cools, and in the process called assembly, the transformation of two-ring clusters into fullerenes take place. Near the surface, the clusters, fullerenes and amorphous structures are condensed, they assemble into associates and in nanoclusters, these nanoclusters form aggregates, which are the microscopic particles of which the soot consists.

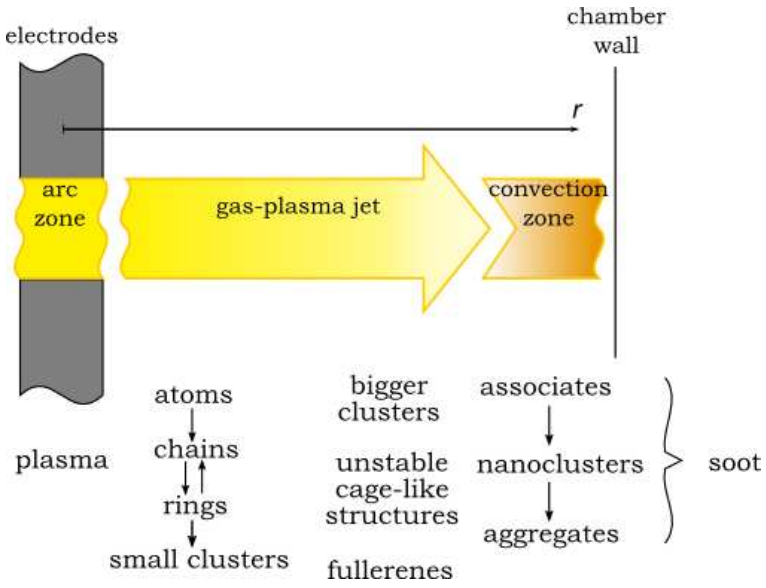

Figure 19: Fullerene formation scheme in arc discharge. For complete description of the fullerene formation, one needs to establish the theory of the arc, the rate of atom condensation and kinetics of carbon clusters in the gas-plasma jet and the description of transformation of smaller polycyclic structures into fullerenes and their associates.

8 Physical model

The model consists of a set of ordinary differential equations describing velocity, temperature and species profiles. In order to solve these equations certain assumptions have to be made. In the next chapter the overview of the assumptions made for one and two-dimensional models is given. Governing equations from different one and two-dimensional models are described in the following subchapters along with the explanation of how the equations are derived from general forms.

8.1 Assumptions

A list of assumptions made by various authors [1], [2] is given below. Not all of the listed assumptions are used in all of the described models. Which assumptions are used in the models described below is specified along the model equations in the following chapters.

- The flow is axisymmetric and laminar with Re < 10.
- The local thermodynamic equilibrium (L.T.E.). A unique temperature is considered to represent plasma. The temperatures of electrons T_e, ions T_i and neutral gas molecules T_g are equal.
- The steady state is assumed when the electrodes are continuously adjusted to keep the inner-electrode gap constant.
- Some models use magnetic field or low gravitational field to optimize the yield.
- The anode erosion rate is uniform over the electrode surface.
- The deposition on the surface of the cathode is governed by diffusion.
- The input of the energy in the arc is due to ohmic heating and to the enthalpy flux of electrons.
- 1D electric field is present in some models.
- The enthalpy diffusion due to species transport is present.
- The radiation losses are accounted for by the net emission coefficient.
- 1D stagnation point flow is used in some of the models.
- Fluid properties are temperature dependent.

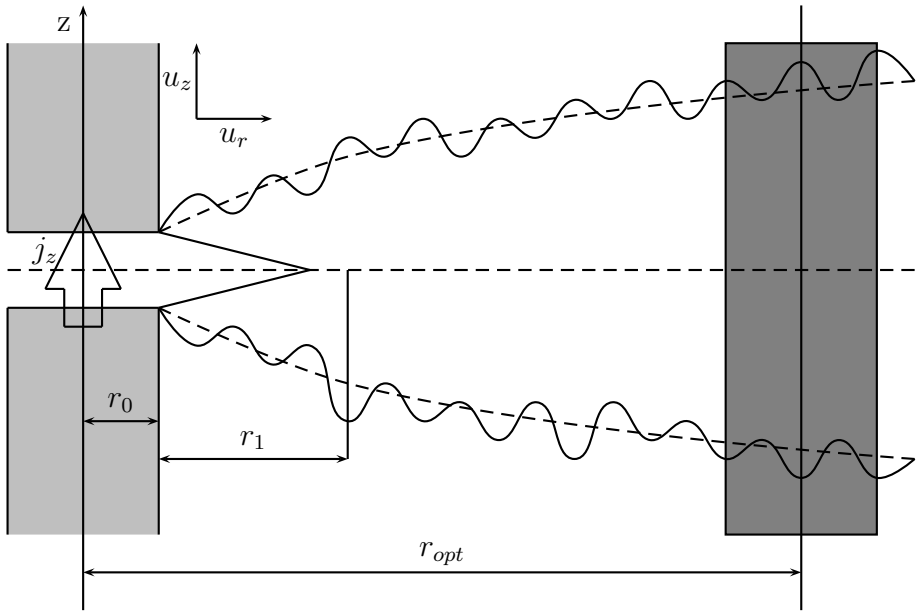

Figure 20: The sketch of the jet fan in the arc-discharge reactor. The arrow depicts the direction of the current flow. r_{opt} is the optimal distance from electrodes to the wall for optimum fullerene formation. The reader should note that the sketch is not done in scale.

8.2 Continuity equation

General continuity equation is normally written in the following form:

$$\frac{D\rho}{Dt} = \frac{\partial \rho}{\partial t} + \vec{\nabla} \cdot (\rho \vec{u}) = S_m \tag{21}$$

where ρ is mass density, $\vec{u}$ the gas velocity and S_m the mass source term. Steady state is assumed if electrodes are continuously adjusted, to maintain the constant inter-electrode gap. We than get [1]

$$\vec{\nabla} \cdot (\rho \vec{u}) = S_m. \tag{22}$$

In 2D cylindrical coordinates the Equation 21 is written as:

$$\frac{\partial \rho}{\partial t} + \frac{1}{r}\frac{\partial}{\partial r}(\rho r u_r) + \frac{\partial}{\partial z}(\rho u_z) = S_m. \tag{23}$$

u_r is radial component of velocity vector $\vec{u}$ and u_z is its axial component. By assuming no mass source we get the formulation of Tanaka [47]:

$$\frac{\partial \rho}{\partial t} + \frac{1}{r}\frac{\partial}{\partial r}(\rho r u_r) + \frac{\partial}{\partial z}(\rho u_z) = 0, \tag{24}$$

and by adding the additional condition of steady state we get the formulation of Dudek [45]:

$$\frac{1}{r}\frac{\partial}{\partial r}(\rho r u_r) + \frac{\partial}{\partial z}(\rho u_z) = 0. \tag{25}$$

For rotating cathode rescaled radial velocity $V = \frac{u_r}{r}$ is inserted into eq. 24 to emphasise the rotating of the cathode. Steady state and $\frac{\partial}{\partial r} \to 0$ are than assumed to get the formulation of Farhat [46]:

$$\frac{\partial \rho}{\partial t} = -\frac{u_z}{\rho}\frac{\partial \rho}{\partial z} - 2V - \frac{\partial u_z}{\partial z} = 0 \tag{26}$$

8.3 Momentum equations

The plasma behaviour in the arc generator is described by the following momentum equation

$$\frac{D(\rho\vec{u})}{Dt} = -\vec{\nabla}P + \vec{\nabla}^2(2\mu\vec{u}) + \vec{\nabla}\cdot(\mu\vec{\nabla}\times\vec{u}) + \rho\vec{g} + \vec{j}\times\vec{B} + \rho\vec{f}, \tag{27}$$

where P is gas pressure, $\vec{g}$ is gravitational acceleration, $\vec{j}$ is current intensity, $\vec{B}$ is magnetic field intensity and $\vec{f}$ vector of body force per unit mass. Equation 27 can be rewritten in cylindrical coordinates as radial and axial momentum equations:

$$\frac{\partial(\rho u_r)}{\partial t} + \frac{1}{r}\frac{\partial}{\partial r}(r\rho u_r^2) + \frac{\partial}{\partial z}(\rho u_r u_z) = -\frac{\partial P}{\partial r} + \frac{1}{r}\frac{\partial}{\partial r}\left(2r\mu\frac{\partial u_r}{\partial r}\right) + \frac{\partial}{\partial z}\left(\mu\frac{\partial u_z}{\partial r} + \mu\frac{\partial u_r}{\partial z}\right) - 2\mu\frac{u_r}{r^2} - j_z B_\theta \tag{28}$$

and

$$\frac{\partial(\rho u_z)}{\partial t} + \frac{1}{r}\frac{\partial}{\partial r}(r\rho u_z u_r) + \frac{\partial}{\partial z}(\rho u_z^2) = -\frac{\partial P}{\partial z} + \frac{\partial}{\partial z}\left(2\mu\frac{\partial u_z}{\partial z}\right) + \frac{1}{r}\frac{\partial}{\partial r}\left(r\mu\frac{\partial u_z}{\partial r} + r\mu\frac{\partial u_r}{\partial z}\right) + \rho g + j_r B_\theta. \tag{29}$$

This equations are used in full form by Tanaka [47] and in a steady state approximation by Dudek [45]. The left part of the equation 27 consists of two parts: time dependent, which represents unsteady acceleration, and spatially dependent term, which represents convective acceleration. On the right side of the same equation, the first term represents pressure gradient, the second describes viscosity, while all the rest of terms describe other bodily forces and can be omitted. In this case gravitation ($\rho\vec{g}$), magnetic field ($\vec{j}\times\vec{B}$) and other unknown forces ($\rho\vec{f}$) are used.

Since industrial plasma behaves, to a good approximation, as a fluid, time dependent and spatial predictions of plasma flow can be made by using classical mechanical equations written bellow.

General momentum equation can be written as:

$$\frac{D(\rho\vec{u})}{Dt} = -\vec{\nabla}P + \mu\vec{\nabla}^2\vec{u} + \rho\vec{g} + \vec{j}\times\vec{B} + \rho\vec{f}. \tag{30}$$

By taking into account that

$$\frac{D\vec{u}}{Dt} = \frac{\partial\vec{u}}{\partial t} + \vec{u}\vec{\nabla}\cdot\vec{u} \tag{31}$$

we get

$$\frac{\partial(\rho\vec{u})}{\partial t} + \vec{\nabla}\cdot(\rho\vec{u}\vec{u}) = -\vec{\nabla}P + \mu\vec{\nabla}^2\vec{u} + \rho\vec{g} + \vec{j}\times\vec{B}. \tag{32}$$

Steady state approximation gives us the following equation [1]:

$$\vec{\nabla}\cdot(\rho\vec{u}\vec{u}) = -\vec{\nabla}P + \mu\vec{\nabla}^2\vec{u} + \rho\vec{g} + \vec{j}\times\vec{B}. \tag{33}$$

By inserting equation 21 into equation 32 with the assumption that there are no mass sources ($S_m = 0$) we get:

$$\rho\frac{\partial\vec{u}}{\partial t} + \rho\vec{u}\vec{\nabla}\cdot\vec{u} = -\vec{\nabla}P + \mu\vec{\nabla}^2\vec{u} + \rho\vec{g} + \vec{j}\times\vec{B} + \rho\vec{f}. \tag{34}$$

Electro-magnetic field in arc plasma cell is described by current intensity $\vec{j}$ and magnetic field intensity $\vec{B}$:

$$\vec{j}\times\vec{B} = (j_r, 0, j_z)\times(B_r, B_\theta, B_z) = \hat{i}(-j_z B_\theta) + \hat{j}(j_z B_r - j_r B_z) + \hat{k}(j_r B_\theta). \tag{35}$$

Due to our 2D geometry only the first and the third terms are allowed. If we rewrite eq. 34 in 2D cylindrical coordinates we get radial momentum:

$$\rho\left(\frac{\partial u_r}{\partial t} + u_r\frac{\partial u_r}{\partial r} + u_z\frac{\partial u_r}{\partial z}\right) = -\frac{\partial P}{\partial r} + \mu\left(\frac{\partial}{\partial r}\left(\frac{1}{r}\frac{\partial}{\partial r}(ru_r)\right) + \frac{\partial^2 u_r}{\partial z^2}\right) + \rho g_r - j_z B_\theta + \rho f_r \tag{36}$$

and axial momentum:

$$\rho\left(\frac{\partial u_z}{\partial t} + u_r\frac{\partial u_z}{\partial r} + u_z\frac{\partial u_z}{\partial z}\right) = -\frac{\partial P}{\partial z} + \mu\left(\frac{1}{r}\frac{\partial}{\partial r}\left(r\frac{\partial u_z}{\partial r}\right) + \frac{\partial^2 u_z}{\partial z^2}\right) + \rho g_z + j_r B_\theta + \rho f_z. \tag{37}$$

1D radial momentum equations for rotating cathode is derived by inserting $f_r = a_r = \frac{u_r^2}{r}$ into eq. 36:

$$\rho\frac{\partial u_r}{\partial t} = -\frac{\partial}{\partial z}\left(\mu\frac{\partial u_r}{\partial z}\right) - \rho u_z\frac{\partial u_r}{\partial z} - \frac{\partial P}{\partial r} - \rho\frac{u_r^2}{r}. \tag{38}$$

By inserting $\frac{u_r}{r} = V$ into eq. 38 we get the formulation of Farhat [46]:

$$\rho\frac{\partial V}{\partial t} = -\frac{\partial}{\partial z}\left(\mu\frac{\partial V}{\partial z}\right) - \rho u_z\frac{\partial V}{\partial z} - \rho V^2 - \frac{1}{r}\frac{\partial P}{\partial r} = 0. \tag{39}$$

8.4 Species conservation equation

General species conservation equation is written as:

$$\frac{D(\rho Y_C)}{Dt} = \vec{\nabla} \cdot (\rho D_C \vec{\nabla} Y_C) + S_{in}, \tag{40}$$

where S_{in} is a negative source term due to condensation and is expressed as a nucleation rate, Y_C is carbon gas-phase fraction and D_C is the diffusional coefficient of carbon species. The right side of Equation 40 describes convection.The first term in the middle of Equation 40 describes diffusion while the second term on the middle of the same equation describes condensation.

Bilodeau [1] gives carbon species conservation equation in a steady state approximation as:

$$\vec{\nabla} \cdot (\rho \vec{v} Y_C) = \vec{\nabla} \cdot (\rho D_C \vec{\nabla} Y_C) + S_{in}. \tag{41}$$

Equation 41 is rewritten in 1D in the following form:

$$\rho \frac{dY_i}{dt} + \frac{\partial(\rho Y_i V_i)}{\partial z} + \rho u \frac{\partial Y_i}{\partial z} = M_i \omega_i \tag{42}$$

In this equation Y_i is a gas-phase species mass fraction, M_i is a molecular weight for species i, V_i is species diffusion velocity and ω_i is chemical production rate of species. Diffusion velocity is calculated in terms of diffusion coefficient and species gradient as written below [48]:

$$V_i = \frac{1}{X_i} D_{im} \frac{dX_j}{dz} - \frac{D_i^T}{\rho Y_i} \frac{1}{T} \frac{dT}{dz}, \tag{43}$$

where D_{im} is:

$$D_{im} = \frac{1 - Y_i}{\sum_{j \neq i}^{K} \frac{X_j}{D_{ji}}}. \tag{44}$$

The second term in Eq. 43 describes thermal diffusion due to Soret effect and can be neglected. In both Equations 43 and 44 X_i stands for mole fraction of the i-th species, D_{im} is the binary diffusion coefficient matrix, D_{ji} is the matrix of ordinal j multicomponent diffusion coefficients, and D_i^T is the thermal diffusion coefficient.

In order to study the time evolution of species mole fraction, diffusion and convection terms in eq. 42 are neglected:

$$\rho \frac{\partial Y_i}{\partial t} = M_i \omega_i. \tag{45}$$

The chemical production rate of the i-th species ω_i can be calculated from the summation of the rate of progress variables q_r for reactions involving the i-th species:

$$\omega_i = \sum_{r=1}^{R} \nu_{ir} q_r = \frac{dC_i}{dt}, \tag{46}$$

where $\nu_{ir} = \nu_{ir}^{''} - \nu_{ir}^{'}$ and

$$q_r = k_{1r} \prod_{i=1}^{n_g} C_i^{\nu_{ir}^{'}} - k_{2r} \prod_{i=1}^{n_g} C_i^{\nu_{ir}^{''}}. \tag{47}$$

$\nu_{ir}^{'}$ and $\nu_{ir}^{''}$ are the stoichiometric mole numbers of reactants and products, respectively, k_{1r} and k_{2r} are forward and reverse rate constants of the r-th reaction and C_i is the molar concentration of the i-th species. Forward k_{1r} and reverse k_{2r} rate constants are calculated from Arrhenius temperature relation:

$$k_{1,2r} = A_{1,2r} T^{\beta_{1,2r}} exp\left(- \frac{E_{1,2}r}{RT} \right), \tag{48}$$

where A_r represents pre-exponential factor, β_r is the temperature exponent and E_r is the activation energy. Indexes 1 and 2 represent forward and reverse direction respectively. Constants A_r, β_r and E_r are taken from the paper of Krestinin and Moravsky [29]. The reactions used in the model are listed in Chapter 8.8.

8.5 Energy equations

The equation for conservation of energy is given by:

$$\frac{D(\rho h)}{Dt} = \vec{\nabla} \cdot (k \vec{\nabla} T) + \frac{\vec{j}^2}{\sigma} + \frac{5}{2} \frac{k_B}{e} \vec{\nabla} \cdot (T \vec{j}) - \vec{\nabla}(k - \rho D_C c_p)(T_C - T_g) \cdot \vec{\nabla} Y_C - 4\pi\varepsilon_n - S_h - U. \tag{49}$$

Specific enthalpy is given by h, c_p represents heat capacity at constant pressure, k thermal conductivity, $\vec{j}$ is current intensity, σ is the electrical conductivity, k_B is Boltzmann's constant, e is the charge of electron, S_h is the enthalpy source term, U is internal energy, ε_n is the net emission coefficient, D_c diffusion coefficient of the carbon species, and T_C and T_g are the temperatures of pure carbon and pure buffer jet respectively. The first term on the right side of the equation 49 represents conduction, the second term describes ohmic heating, while the rest of the terms are optional and represent enthalpy flux of electrons $\frac{5}{2}\frac{k_B}{e}\vec{\nabla} \cdot (T\vec{j})$, enthalpy diffusion due to species transport $\vec{\nabla}(k - \rho D_C c_p)(T_C - T_g) \cdot \vec{\nabla} Y_C$, radiational losses $4\pi\varepsilon_n$, enthalpy sources S_h and internal energy U. The current intensity is connected with the electric field by the following equation $\vec{j} = \sigma \vec{E}$. Energy equation (49) in cylindrical form is expressed as:

$$\frac{\partial(\rho h)}{\partial t} + \frac{1}{r}\frac{\partial}{\partial r}(r \rho u_r h) + \frac{\partial}{\partial z}(\rho u_z h) = \frac{1}{r}\frac{\partial}{\partial r}\left(r k \frac{\partial T}{\partial r} \right) + \frac{\partial}{\partial z}\left(k \frac{\partial T}{\partial z} \right) + \frac{j_r^2 + j_z^2}{\sigma} - U \tag{50}$$

By inserting enthalpy temperature relation $\vec{\nabla}h = k\vec{\nabla}T$ into steady state equation 49 and adding two additional terms, Dudek [45] derived the following equation:

$$\frac{1}{r}\frac{\partial}{\partial r}(\rho r u_r h)+\frac{\partial}{\partial z}(\rho u_z h) = \frac{1}{r}\frac{\partial}{\partial r}\left(\frac{rk}{c_p}\frac{\partial h}{\partial r}\right)+\frac{\partial}{\partial z}\left(\frac{k}{c_p}\frac{\partial h}{\partial z}\right)+\left(\frac{j_r^2+j_z^2}{\sigma}-S_t+\frac{5}{2}\frac{k_B}{e}\left(\frac{j_r}{c_p}\frac{\partial h}{\partial r}+\frac{j_z}{c_p}\frac{\partial h}{\partial z}\right)\right). \tag{51}$$

The first additional term is radiational loss per velocity S_t, while the second additional term describes heating and cooling effects from electron flow $\frac{5}{2}\frac{k_B}{e}(\frac{j_r}{c_p}\frac{\partial h}{\partial r}+\frac{j_z}{c_p}\frac{\partial h}{\partial z})$. We derive this term from the following equation

$$\frac{5k_B\vec{\nabla}\cdot(T\vec{j})}{2e} = \frac{5}{2}\frac{k_b}{e}(\vec{j}\cdot\vec{\nabla}T + T\vec{\nabla}\cdot\vec{j}), \tag{52}$$

where $\frac{5}{2}k_BT$ is electron specific heat. By taking into account the enthalpy temperature relation $\vec{\nabla}h = c_p\vec{\nabla}T$ and the current continuity equation

$$\vec{\nabla}\cdot\vec{j} = \frac{1}{r}\frac{\partial}{\partial r}(rj_r)+\frac{\partial}{\partial z}(j_z) = 0 \tag{53}$$

we get

$$\frac{5k_B\vec{\nabla}\cdot(T\vec{j})}{2e} = \frac{5}{2}\frac{k_b}{c_pe}\left(j_z\frac{\partial h}{\partial z}+j_r\frac{\partial h}{\partial r}\right). \tag{54}$$

As mention in a previous subsection (8.3), industrial plasma behaves, to a good approximation, as a fluid. Thus time dependent and spatial predictions of plasma flow are made by using classical mechanical equations. Bilodeau [1] added net emission coefficient ε_n term to consider radiation losses, enthalpy source term S_h, and species transport term to consider enthalpy diffusion. He also assumed 1D electric field. Energy conservation equation is than written as:

$$\vec{\nabla}\cdot(\rho\vec{v}h) = \vec{\nabla}\cdot(k\vec{\nabla}T)+\frac{j_z^2}{\sigma}+\frac{5}{2}\frac{k_b}{e}c_p\vec{j}\cdot\vec{\nabla}T-\vec{\nabla}(k-\rho D_C c_p)(T_C-T_g)\cdot\vec{\nabla}Y_C-4\pi\varepsilon_n+S_h. \tag{55}$$

By omitting the effects of electron flow in Equation 55, we get 1D steady state energy equation used by Farhat [46]:

$$\rho c_p\frac{\partial T}{\partial t} = \frac{\partial}{\partial z}\left(k\frac{\partial T}{\partial z}\right)-\rho c_p u_r\frac{\partial T}{\partial z}-\sum_{i=1}^{n_g}\left(c_{pi}\rho Y_i V_i\frac{\partial T}{\partial r}+\omega_i h_i\right)+S_q-Q_{rad} = 0. \tag{56}$$

The radiative term Q_{rad} accounts for the net loss of energy by gas radiation, the source term S_q accounts for the electrical energy dissipated in the arc, ω_i is the net chemical production rate of species i by gas-phase reaction and Y_i gas-phase species mass fraction.

8.6 Equation of state

Another equation that is used to describe the fullerene synthesis in the arc discharge method is the equation of state:

$$P = \frac{\rho RT}{M}, \tag{57}$$

where R is the universal gas constant, P is gas pressure, ρ is mass density, T is the temperature and M is molecular weight.

8.7 Boundary conditions

Boundary conditions consist of physical boundaries of the model as well as conditions imposed within the domain. Physical boundaries include dimensions of the reactor cell (length, width (2D model)), cathode and anode length, and the size of the inter-electrode gap.

Wall and anode tip (side and axis) temperature are given as boundary conditions whereas cathode tip temperature can be given (in the case of Bilodeau [1]) or predicted (Farhat [46]) as a part of solution, if a radiative energy balance is added:

$$k\frac{\partial T}{\partial x}\bigg|_{cathode} = \sigma\varepsilon(T_C^4 - T_A^4). \tag{58}$$

T_A is the anode temperature, T_C is the cathode temperature, ε is the surface emissivity and σ is the Stefan-Boltzman constant.

In the inter-electrode region anode surface area A, total gas density ρ and measured erosion rate Φ are parameters from which the axial gas velocity from the anode u_A:

$$u_A = \frac{\Phi}{\rho A} \tag{59}$$

is estimated by Farhat [2]. The radial velocity is zero. The same can be claimed for axial velocity at the stagnation flow point. Both radial and axial velocities are zero at the wall surface $u_r = u_z = 0$.

We impose the $X_C = 0$ condition on the wall, since carbon vapour pressure is negligible near the reactor wall. Along the axis the following conditions are true:

$$\frac{\partial T}{\partial r} = \frac{\partial X_C}{\partial r} = \frac{\partial V}{\partial r} = \frac{\partial J_z}{\partial r} = 0. \tag{60}$$

At equilibrium temperature T_A, mass fractions can be calculated from a dilution fraction:

$$\tau = \frac{M_C + M_{Ni} + M_Y}{M_C + M_{Ni} + M_Y + M_{He\ or\ Ar}} \times 100, \tag{61}$$

which accounts for the mixing of the anode material with an inert atmosphere. M_C, M_{Ni}, M_Y and $M_{He\ or\ Ar}$ are molecular weights of carbon, nickel, iridium and either helium or argon.

In the case of modelling nanotube growth (Bilodeau [1]) a set of surface reactions simulating nanotube growth has to be considered. The theoretical number of nanotube sites Γ:

$$\Gamma = \frac{3N_{at}}{3\sqrt{3}(d_{CNT} + d_{NT-TN})^2} \times \frac{1}{N_{A_V}} \tag{62}$$

is assumed to be conserved. The surface species conservation equation is given by:

$$\frac{dZ_{CR}}{dt} = \frac{s_{CR}}{\Gamma} = 0, \tag{63}$$

where Z_{CR} is surface species site fraction and s_{CR} is the chemical production of surface species. We can than calculate nanotube growth rate G from the following equation:

$$G = \frac{s_{CR} M_{CNT}}{\rho_{CNT}}, \tag{64}$$

where ρ_{CNT} is nanotube bulk mass density and M_{CNT} is molecular weight.

8.8 Chemical reactions

The chemical kinetics model is based on the fullerene growth model, which assumes the formation of clusters of carbon from atoms to carbon chains, rings and polycycles, fullerene shells, to C_{60} and C_{70}, and than soot, which is assumed to have 80 atoms in the present model. The chemical reactions of a full model are listed in Table 1.

Chemistry of small clusters (C_1 - C_{10})
$C+C \leftrightarrow C_2$
$C+C_2 \leftrightarrow C_3$
$C_2+C_2 \leftrightarrow C_3+C$
$C_2+C_2 \leftrightarrow C_4$
$C_1+C_3 \leftrightarrow C_4$
$C_1+C_4 \leftrightarrow C_5$
$C_2+C_3 \leftrightarrow C_5$
$C_{n-m}+C_m \leftrightarrow C_n$
$6 \leq n \leq 10$ and $1 \leq m \leq \frac{n}{2}$
Chemistry of cycles and polycycles (C_{11} - C_{31})
$C_{n-m}+C_m \leftrightarrow C_n$
$11 \leq n \leq 31$ and $1 \leq m \leq 15$

Formation of fullerenes

$C_{n-m}+C_m \leftrightarrow C_n$

$32 \leq n \leq 46$ and $n - 31 \leq m \leq 15$

Growth of fullerene shells

$C_n+C \leftrightarrow C_{n+1}$

$32 \leq n \leq 78$, $n \neq 59$ and $n \neq 69$

$C_n+C_2 \leftrightarrow C_{n+2}$

$32 \leq n \leq 77$, $n \neq 58$ and $n \neq 68$

$C_n+C_3 \leftrightarrow C_{n+2}+C$

$32 \leq n \leq 77$

Formation and decay of fullerene molecules C_{60}^F and C_{70}^F

$C_{60} \rightarrow C_{60}^F$

$C_{59}+C \rightarrow C_{60}^F$

$C_{58}+C_2 \leftrightarrow C_{60}^F$

$C_{58}+C_3 \rightarrow C_{60}^F+C$

$C_{60}^F+C \rightarrow C_{61}$

$C_{60}^F+C_2 \rightarrow C_{62}$

$C_{60}^F+C_3 \rightarrow C_{63}$

$C_{70} \rightarrow C_{70}^F$

$C_{69}+C \rightarrow C_{70}^F$

$C_{68}+C_2 \leftrightarrow C_{70}^F$

$C_{68}+C_3 \rightarrow C_{70}^F+C$

$C_{70}^F+C \rightarrow C_{71}$

$C_{70}^F+C_2 \rightarrow C_{72}$

$C_{70}^F+C_3 \rightarrow C_{72}+C$

Formation of soot nuclei Z

$C_{76}+ C_2 \rightarrow Z$

$C_{78}+C_2 \rightarrow Z + C$

$C_{60-m}+C_{60-n} \rightarrow Z$

$C_{70-m}+C_{70-n} \rightarrow Z$

$1 \leq n - m \leq 10$

Heterogeneous reactions on soot particles

$C_1 + \text{soot} \leftrightarrow \text{soot}$

$C_2 + \text{soot} \leftrightarrow \text{soot}$

$C_3 + \text{soot} \leftrightarrow \text{soot}$

$C_n + \text{soot} \leftrightarrow \text{soot}$

$4 \leq n \leq 79$

$C_{60}^F + \text{soot} \leftrightarrow \text{soot}$

C_{70}^F + soot $\leftrightarrow$ soot

Table 1: Chemical reactions [29].

By considering the complexity of the problem, the full chemical model is reduced since it is computationally too expensive [11]. This is done by combining or eliminating species and their corresponding reactions. High reaction rates and consequently short times for carbon cluster formation allow for this reduction. List of chemical reactions used to calculate species concentrations in Equation 47 is given in Table 1.

Chemistry of small clusters
$C+C \leftrightarrow C_2$
$C+C_2 \leftrightarrow C_3$
$C_2+C_2 \leftrightarrow C_3+C$
Formation of carbon clusters CC
$C_3+C \leftrightarrow 0.100$ CC
$C_3+C_2 \leftrightarrow 0.125$ CC
$C_3+C_3 \leftrightarrow 0.150$ CC
Growth of carbon clusters CC
$CC+C \leftrightarrow 1.025$ CC
$CC+C_2 \rightarrow 1.050$ CC
$CC \rightarrow 0.95$ CC + C
Formation of fullerene molecules C_{60}^F and C_{70}^F
$CC+C_3 \rightarrow 0.70\ C_{60}^F$
$CC+C_2 \rightarrow 0.70\ C_{60}^F$
$CC+C \rightarrow 0.6833333\ C_{60}^F$
Decay of fullerene molecules C_{60}^F and C_{70}^F
$C_{60F} \rightarrow 1.45$ CC + C_2
$C_{70F} \rightarrow 1.70$ CC + C_2
Formation of soot nuclei Z and growth of soot
$CC+CC \rightarrow Z$
$Z+C_3 \rightarrow 1.0375$ Z
$Z+C_2 \rightarrow 1.025$ Z
$Z+C \rightarrow 1.0125$ Z

Table 2: Reduced chemical model [11].

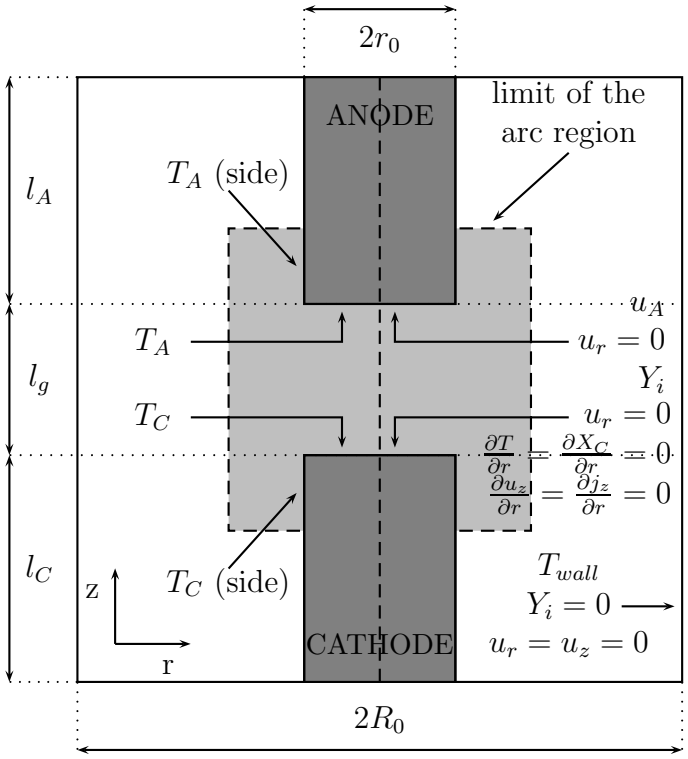

Figure 21: Boundary conditions [1].

9 The model

Two models are proposed for fullerene production. The initial one-dimensional model is based on Farhat et al. [2] formulation whereas the improved model is based on Bilodeau et al. [1] two-dimensional model.

9.1 The initial model

Our initial model consists of four basis 1D equations: continuity equation, momentum, energy and species conservation equations. The equations were taken from Farhat model [46] with the assumption that the cathode is not rotating and that the magnetic field is present. The continuity equation is than written in the following form:

$$\frac{\partial \rho}{\partial t} = -\frac{u_z}{\rho}\frac{\partial \rho}{\partial z} - \frac{\partial u_z}{\partial z} = 0. \tag{65}$$

In the radial momentum equation (Eq. 39) the term describing the rotation of the cathode was left out due to the assumption that the cathode does not rotate and the term describing magnetic field was added:

$$\rho\frac{\partial u_r}{\partial t} = -\frac{\partial}{\partial z}\left(\mu\frac{\partial u_r}{\partial z}\right) - \rho u_z\frac{\partial u_r}{\partial z} - \frac{\partial p}{\partial r} - j_z B_\theta. \tag{66}$$

To the energy equation (eq. 56) the current term $\frac{j_z^2}{\sigma}$ and the electron-enthalpy term $\frac{5}{2}\frac{k_b}{e}j_r\frac{\partial T}{\partial r}$ are added, while the radiative and enthalpy source terms are omitted:

$$\rho c_p\frac{\partial T}{\partial t} = \frac{\partial}{\partial z}\left(k\frac{\partial T}{\partial z}\right) - \rho c_p u_r\frac{\partial T}{\partial z} - \sum_{i=1}^{n_g}\left(c_{pi}\rho Y_i V_i\frac{\partial T}{\partial r} + \omega_i h_i\right) + \frac{j_z^2}{\sigma} + \frac{5}{2}\frac{k_b}{e}j_r\frac{\partial T}{\partial r} = 0. \tag{67}$$

The same species conservation equation as in Farhat model (eq. 45 [46]) is used:

$$\rho\frac{dY_i}{dt} = M_i\omega_i. \tag{68}$$

The following boundary conditions are going to be used: the geometry of the reactor cell (width, length, cathode and anode radius and length), cathode and anode temperature, radial and axial velocities at the anode an at the wall surface, $X_C = 0$ condition at the wall, and $\frac{\partial T}{\partial r} = \frac{\partial X_C}{\partial r} = \frac{\partial V}{\partial r} = \frac{\partial J_z}{\partial r} = 0$ conditions along the axis.

9.2 Planed improvements

Once the initial model is working properly it is going to be extended to two dimensions. Again, four basic equations are going to be used. The continuity equation will be taken from Bilodeau model [1]:

$$\vec{\nabla}\cdot(\rho\vec{v}) = S_m \tag{69}$$

and re-written in cylindrical coordinates:

$$\frac{1}{r}\frac{\partial}{\partial r}(\rho r u_r) + \frac{\partial}{\partial z}(\rho u_z) = S_m. \tag{70}$$

The same is going to be applied to the momentum equation (Eq. 33) to get the radial momentum (Eq. 36):

$$\rho\left(\frac{\partial u_r}{\partial t} + u_r\frac{\partial u_r}{\partial r} + u_z\frac{\partial u_r}{\partial z}\right) = -\frac{\partial p}{\partial r} + \mu\left(\frac{\partial}{\partial r}\left(\frac{1}{r}\frac{\partial}{\partial r}(r u_r)\right) + \frac{\partial^2 u_r}{\partial z^2}\right) + j_z B_\theta \tag{71}$$

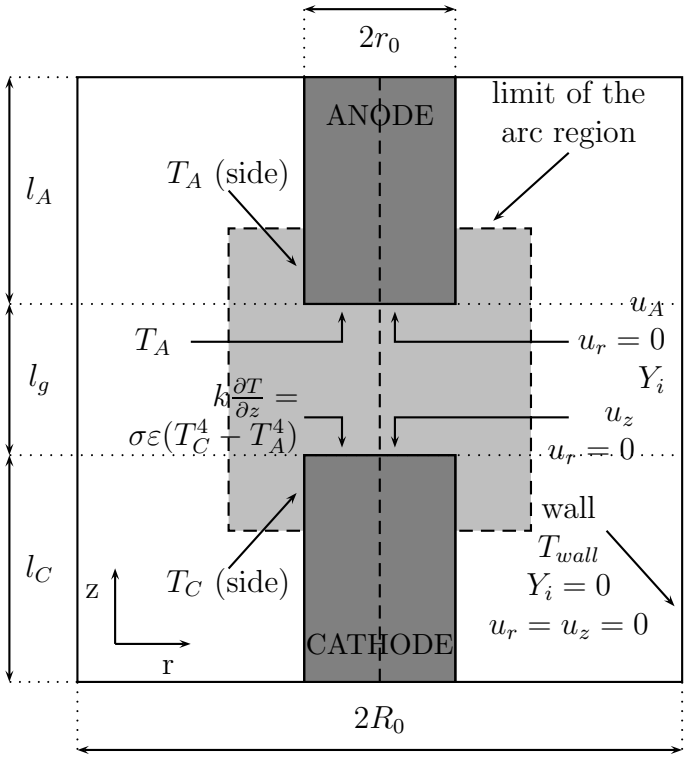

Figure 22: Boundary conditions for one-dimensional model.

and the axial momentum (Eq. 37):

$$\rho\left(\frac{\partial u_z}{\partial t} + u_r\frac{\partial u_z}{\partial r} + u_z\frac{\partial u_z}{\partial z}\right) = -\frac{\partial p}{\partial z} + \mu\left(\frac{1}{r}\frac{\partial}{\partial r}\left(r\frac{\partial u_z}{\partial r}\right) + \frac{\partial^2 u_z}{\partial z^2}\right) + \rho g_z + j_r B_\theta. \tag{72}$$

Energy equation is going to be written in the following form:

$$\vec{\nabla}\cdot(\rho\vec{v}h) = \vec{\nabla}\cdot(k\vec{\nabla}T) + \frac{j_z^2}{\sigma} + \frac{5}{2}k_b\vec{j}\cdot\vec{\nabla}T - 4\pi\varepsilon_n + S_n - \vec{\nabla}\cdot(k - \rho D_C c_p)(T_C - T_g)\vec{\nabla}Y_C \tag{73}$$

which gives us the specified equation in cylindrical coordinates:

$$\frac{1}{r}\frac{\partial}{\partial r}(r\rho u_r h) + \frac{\partial}{\partial z}(\rho u_z h) = \frac{1}{r}\frac{\partial}{\partial r}\left(rk\frac{\partial T}{\partial r}\right) + \frac{\partial}{\partial z}\left(k\frac{\partial T}{\partial z}\right) + \frac{j_z^2}{\sigma} + \tag{74}$$

$$+ \frac{5}{2}\frac{k_b}{e}\left(j_r\frac{\partial T}{\partial r} + j_z\frac{\partial T}{\partial z}\right) - \tag{75}$$

$$- \frac{1}{r}\frac{\partial}{\partial r}(rk - r\rho D_C c_p)(T_C - T_g)\frac{\partial Y_C}{\partial r} - \tag{76}$$

$$- \frac{\partial}{\partial z}(k - \rho D_C c_p)(T_C - T_g)\frac{\partial Y_C}{\partial z}. \tag{77}$$

Species conservation equation is going to be taken from Bilodeau model [1]:

$$\vec{\nabla}\cdot(\rho\vec{u}Y_C) = \vec{\nabla}\cdot(\rho D_C\vec{\nabla}Y_C) + S_{in} \tag{78}$$

which gives us the specified equation in cylindrical coordinates:

$$\rho\frac{\partial Y_C}{\partial t} + \frac{1}{r}\frac{\partial}{\partial r}(r\rho u_r Y_C) + \frac{\partial}{\partial z}(\rho u_z Y_C) = \frac{1}{r}\frac{\partial}{\partial r}\left(r\rho u_r\frac{\partial Y_C}{\partial r}\right) + \frac{\partial}{\partial z}\left(\rho u_z\frac{\partial Y_C}{\partial z}\right) + S_{in}. \tag{79}$$

The following boundary conditions are going to be applied: the geometry of the reactor cell (width, length, cathode and anode radius and length), cathode and anode temperature, radial and axial velocities at the anode an at the wall surface, $X_C = 0$ condition at the wall, and $\frac{\partial T}{\partial r} = \frac{\partial X_C}{\partial r} = \frac{\partial V}{\partial r} = \frac{\partial J_z}{\partial r} = 0$ conditions along the axis.

9.3 Typical values of material constants

To better characterize the conditions in the arc-discharge reactor, typical parameter values are taken from [1], [2] and are listed in the Table 3. The measurements were made in two different reactor chambers for two noble gasses; namely argon (Ar) and helium (He). The values for each reactor chamber are within limits given in the Table 3. The parameters with the specific values were only measured for one of the reactors.

Input parameters		
constant	**label**	**value**
anode diameter	$2r_A$	6 - 7 mm
cathode diameter	$2r_C$	6 - 16 mm
anode length	l_A	15-70 cm
anode hole diameter		3 mm

anode hole depth		100 mm
cathode length	l_C	15 -30 cm
reactor length	$l_C + l_A + l_g$	39-100 cm
reactor diameter	$2r$	13.6-30 cm
current	I	60-100 A
pressure	P	100-800 mbar
anode cathode distance	l_g	1-12 mm
anode tip temperature	T_A	3300-3800 K
anode side temperature	$T_{A(side)}$	2800-3300 K
cathode tip temperature	T_C	3300-3800 K
cathode side temperature	$T_{C(side)}$	2800-3300 K
wall temperature	T_w	350 K
mass density of the gas	ρ	$9.24 \cdot 10^{-6} \frac{\mathrm{g}}{\mathrm{cm}^3}$
anode surface area	A	0.29 cm^2
pre-exponential factor	A	$2.5 \cdot 10^{11} - 1 \cdot 10^{13}$
carbon mass fraction	n_C	$10^{-4} - 10^{-6}$
initial C mole fraction	N_C	$02.57 \cdot 10^{-4}$
initial C_2 mole fraction	N_{C_2}	0.583
initial C_3 mole fraction	N_{C_3}	0.379
initial Ni mole fraction	N_{Ni}	0.0386
current intensity	j	$3 \cdot 10^6 - 10^7 \frac{\mathrm{A}}{\mathrm{m}^2}$
Output parameters		
constant	**label**	**value**
anode gas velocity	u_A	$7818 \frac{\mathrm{cm}}{\mathrm{s}}$
deposition rate		$0.57 - 4.71 \frac{\mathrm{mg}}{\mathrm{s}}$
electric power dissipation	q	$1.24 \cdot 10^7 \frac{\mathrm{W}}{\mathrm{m}^2}$
dilution factor at the anode	τ	20
erosion rate	Φ	$1.3 - 25 \cdot 10^{-3} \frac{\mathrm{g}}{\mathrm{s}}$
estimated electron density	N_e	$3.5 \cdot 10^{15} \frac{1}{\mathrm{cm}^3}$
temperature	T	350-17000 K
He number density	n_{He}	$1.4 \cdot 10^{18} \frac{1}{\mathrm{cm}^3}$
Ni number density	n_{Ni}	$2.0 \cdot 10^{14} \frac{1}{\mathrm{cm}^3}$
Y number density	n_Y	$3.2 \cdot 10^{14} \frac{1}{\mathrm{cm}^3}$
growth rate		$1 - 1000 \frac{\mu\mathrm{m}}{\mathrm{min}}$

Table 3: Typical parameter values as reported in the papers of Farhat and Bilodeau [1], [46].

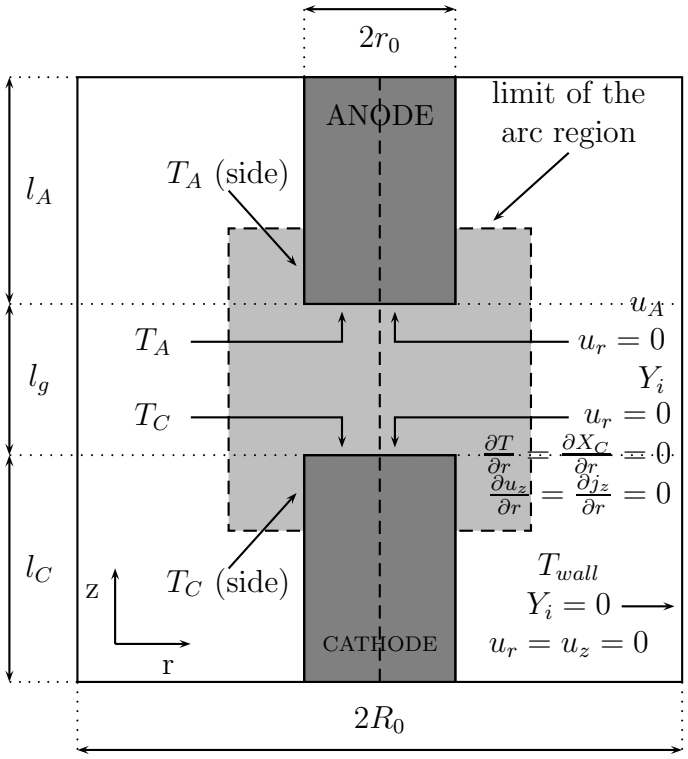

Figure 23: Boundary conditions for two-dimensional improved model.

9.4 Estimated parameter fields

To effectively portray the environment in the arc-discharge reactor, temperature, carbon mass fraction and axial current velocity gradient field estimations are drawn in Figures 24, 25 and 26. The estimations were made based on Bilodeau calculations [1]. Left graph shows the parameter profile in the whole reactor cell, while the right graph depicts only the expected parameter field inside the inter electrode region.

10 The numerical solutions of the governing equations

Both, the initial and the improved model are going to be solved numerically with a mesh-reduction technique otherwise known as mesh-less method. That is a numerical simulation

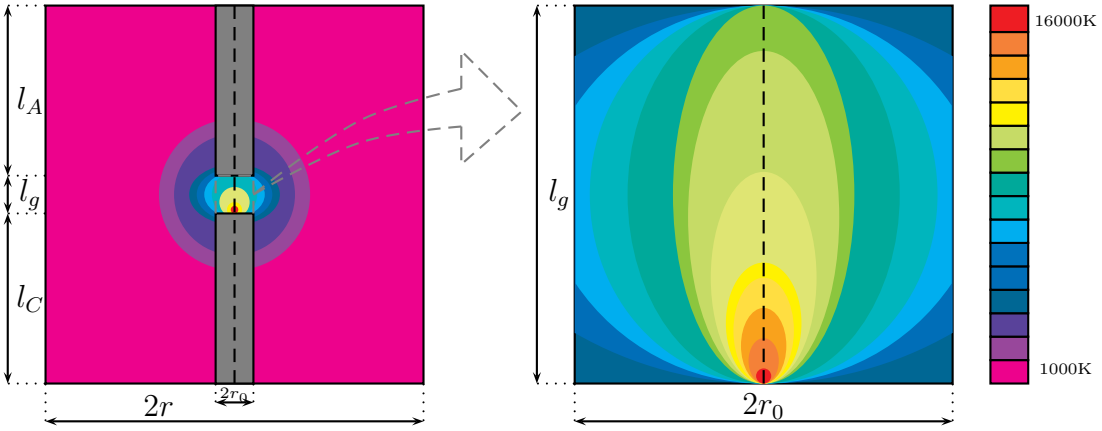

Figure 24: Temperature estimation

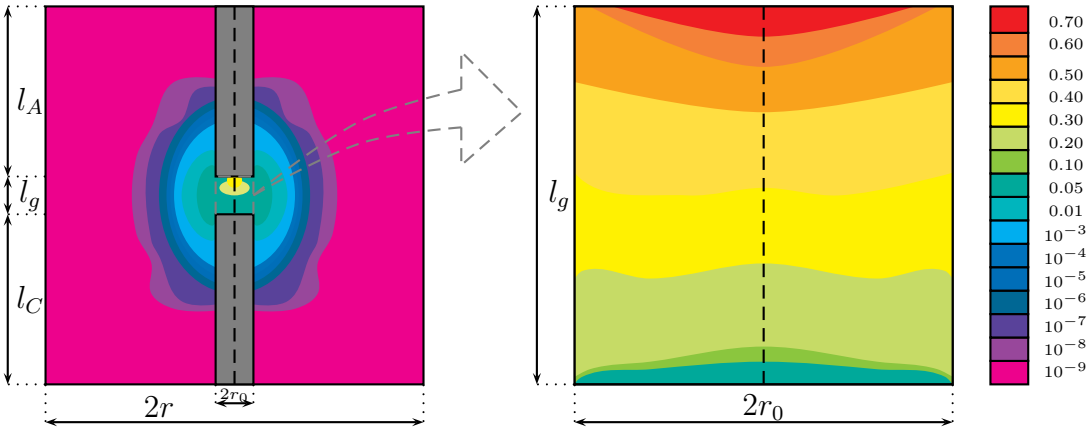

Figure 25: Estimated profiles of carbon mass fraction.

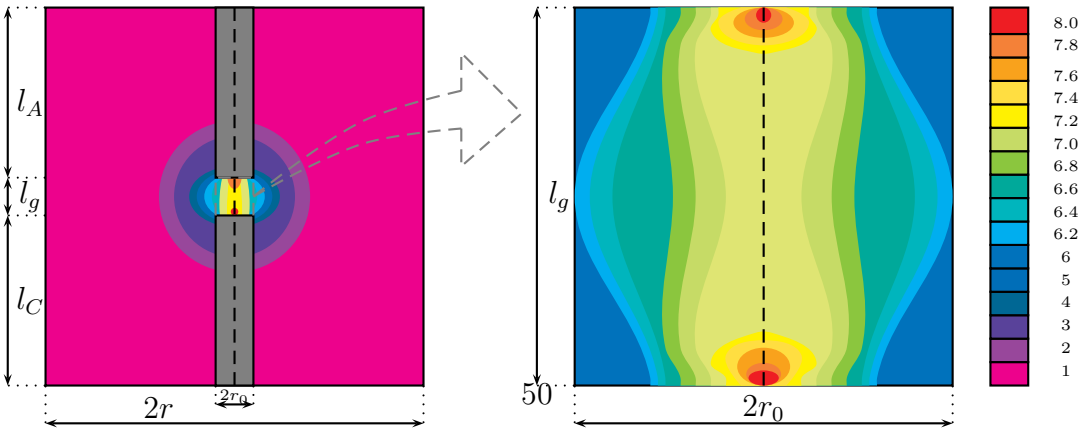

Figure 26: Axial current intensity estimation.

algorithm that uses a set of arbitrary distributed nodes both within the problem domain and on its boundary to represent the solution of a physical phenomena. The radial basis function collocation method (RBFCM) [49] is the simplest mesh-free method among the number of meshless methods developed to solve temperature and fluid flow equations. Its local version (LRBFCM) developed by Šarler and Vertnik [50], described in Chapter 10.2, will be implemented in numerical approximation.

10.1 Radial basis function

Radial basis functions (RBFs) are general approximation functions of univariate polynomial splines to a multivariate domain. The RBFs [12] can be expressed in the following form

$$\psi_i(r) = \psi(\vec{p} - \vec{p}_i), \tag{80}$$

where r, which is defined by the Euclidian norm

$$r = ||\vec{p} - \vec{p}_i|| = \sqrt{(\vec{p} - \vec{p}_i) + (\vec{p} - \vec{p}_i)}, \tag{81}$$

is the radial distance between the position vector $\vec{p}$ and reference position vector $\vec{p}_i$, both of which are radially symmetric and thus independent of any kind of rotation. The most commonly used RBF forms are [12]:

- Gaussian (GA)
$$\psi(r) = e^{-(cr)^2}, \tag{82}$$
- multiquadric (MQ),
$$\psi(r) = \sqrt{r^2 + c^2}, \tag{83}$$
- inverse multiquadric (IMQ)
$$\psi(r) = \frac{1}{\sqrt{r^2 + c^2}}, \tag{84}$$
- thin plane spline (TPS)
$$\psi(r) = \left(\frac{r}{c}\right)^2 \log\left(\frac{r}{c}\right), \tag{85}$$

where c stands for free parameter, which has to either be predetermined or set as a part of the solution. In the instance of our model any radial function that is twice differentiable would be appropriate. A general form of approximation function Θ is than represented as a linear combination of RBFs centred at points $\vec{p}_i$:

$$\Theta(\vec{p}) = \sum_{i=1}^{N} \alpha_i \psi_i(\vec{p}), \tag{86}$$

where N stands for a number of points and α_i for an expansion coefficient.

10.2 Local radial basis function collocation method

The idea behind the local radial basis function collocation method (LRBFCM) is to approximate a function locally over a set of neighbouring nodes [12]. The RBFs are used as a basis and the collocation is used for the determination of the coefficients.

In order to approximate the function Θ, the value of which is only known for a set of points, RBF interpolation is used. For a given set of N distinct data points $\vec{p}_1, \ldots, \vec{p}_N$, corresponding data values $\theta_1, \ldots, \theta_N$ and a set of radial basis functions $\psi_1, \ldots, \psi_N$ [12], the interpolation is given by

$$\Theta(\vec{p}) \approx \sum_{i=1}^{N} \alpha_i \psi_i(\vec{p}). \tag{87}$$

By considering the collocation condition

$$\Theta(\vec{p}_i) = \theta_i, \tag{88}$$

we get a linear system of N equations:

$$\mathbf{\Psi}\vec{\alpha} = \vec{\theta}, \tag{89}$$

where the components of basis matrix $\mathbf{\Psi}$ are introduced as

$$\Psi_{ij} = \psi\big(||\vec{p}_i - \vec{p}_j||\big). \tag{90}$$

The expansion coefficients α_i can only be determined when the number of domain nodes matches the number of the basis functions and when the basis functions matrix is non-singular [12]. The coefficients are than computed from

$$\vec{\alpha} = \mathbf{\Psi}^{-1}\vec{\theta}. \tag{91}$$

In order to be able to solve the partial differential equations of the model, first and second derivative of function $\Theta(\vec{p})$ must be calculated on the influence domain. The operator applied on the approximated function is expressed by [53]:

$$\frac{\partial^i}{\partial p_\iota^i}\Theta(\vec{p}) = \sum_{n=1}^{N} \alpha_n \frac{\partial^i}{\partial p_\iota^i}\Psi_n(\vec{p}), \tag{92}$$

where the index ι is used to denote coordinates.

To calculate initial and improved model first and second derivatives are used. Once and twice derived RBFs of the most common basis functions are given as:

- GA

$$\frac{\partial}{\partial p_\iota}\Psi(r) = 2c^2 r e^{-(cr)^2} \qquad and \qquad \frac{\partial^2}{\partial p_\iota^2}\Psi(r) = 2c^2(-1+2c^2r^2)\Psi(r), \tag{93}$$

- MQ

$$\frac{\partial}{\partial p_\iota}\Psi(r) = \frac{p_\iota - p_{\iota i}}{\Psi(r)} \qquad and \qquad \frac{\partial^2}{\partial p_\iota^2}\Psi(r) = -\frac{p_\iota - p_{\iota i}}{\Psi^3(r)}, \tag{94}$$

- IMQ

$$\frac{\partial}{\partial p_\iota}\Psi(r) = -(p_\iota - p_{\iota i})\Psi^3(r) \qquad and \qquad \frac{\partial^2}{\partial p_\iota^2}\Psi(r) = -3\Psi^2(r), \tag{95}$$

- TPS

$$\frac{\partial}{\partial p_\iota}\Psi(r) = \frac{r}{c} + \frac{2r}{c^2}\log\frac{r}{c} \qquad and \qquad \frac{\partial^2}{\partial p_\iota^2}\Psi(r) = \frac{p_\iota - p_{\iota i}}{c}\left(1 + \frac{2}{c}\log\frac{r}{c}\right). \tag{96}$$

10.3 Boundary conditions

There are three types of boundary conditions commonly used for solving partial differential equations in the transport equation context; Dirichlet, Neuman and Robin. The boundary conditions are given as [53]:

- Dirichlet

$$\Theta(\vec{p}) = \Theta_{BC}, \tag{97}$$

- Neuman

$$\frac{\partial}{\partial \vec{n}}\Theta(\vec{p}) = \Theta_{BC}, \tag{98}$$

- Robin

$$a\frac{\partial}{\partial \vec{n}}\Theta(\vec{p}) + b\Theta(\vec{p}) = \Theta_{BC}, \tag{99}$$

where a and b are constants, $\vec{n}$ is normal vector and Θ_{BC} is the value of boundary condition. While the implementation of Dirichlet boundary condition, which specifies the value of the function on the surface, is straightforward, collocation has to be used in order to satisfy the Neuman and Robin conditions. The boundary values are computed from

$$\Theta_{BC} = \sum_{i=1}^{N} \alpha_i \frac{\partial}{\partial \vec{n}}\Psi_i(\vec{p}) \tag{100}$$

for Neuman boundary condition and from

$$\Theta_{BC} = \sum_{i=1}^{N} \alpha_n \left(a \frac{\partial}{\partial \vec{n}} \Psi_i(\vec{p}) + b \Psi_i(\vec{p}) \right) \tag{101}$$

for Robin boundary condition.

To solve initial as well as improved model presumably only Dirichlet and Neuman boundary conditions will be used.

11 Conclusion

Since the discovery of buckyballs in 1980s and nanotubes in the following years, the fullerene family has garnered a lot of attention in scientific circles, due to the unique properties of the material and wide range of possible applications. Among the numerous production techniques the arc discharge method and its variations have proven the most effective. Nevertheless, the maximum yield is still relatively low, thus making the material one of the most expensive in the world. In order to improve the yield and consequently reduce the cost of fullerenes, several attempts have been made to formulate a mathematical model describing physical phenomena behind the fullerene formation. Since the process that governs the fullerene formation is not yet completely understood, because of the big amount of parameters involved in the process, the final model still has to be developed. Even so, some of the existing models are in good agreement with experimental data.

To avoid the meshing problems that might arise when solving the equations numerically, the mesh-reduction or mesh-less method is going to be used. Its biggest advantage is in its feature, specifying that the solution can be described on the erratically distributed nodes. The LRBFM is promising mesh-less technique that is going to be used to explore the solutions in this case. When implemented into the numerical code, the models are able to predict temperature and current field, species distribution, fulleren yield and growth rate.

In this paper a brief introduction to fullerene production is presented along with a review of fullerene models described in literature. The formulation of mathematical model suggested to be used in numerical calculations is given as well as the description of method proposed for solving the model's equations.

A Additional equations

$$\sum_{i=1}^{n_s} \nu_{ir}^{'} A_i \overset{1}{\underset{2}{\rightarrow}} \sum_{i=1}^{n_s} \nu_{ir}^{''} A_i \tag{102}$$

$$\sum_{i=1}^{n_s} Y_i = 1 \tag{103}$$

$$E = \frac{I}{G} = \frac{I}{2\pi \int_0^R \sigma r dr} \tag{104}$$

$$B = \frac{\mu_0}{R} \int_0^R J_r dr \tag{105}$$

$$S_q(x) = q \frac{1}{w_s} \sqrt{\frac{3}{\pi}} e^{\frac{-3(x-x_s)^2}{w_s^2}} \tag{106}$$

$$q = \int_{-w_s}^{+w_s} S_q(x) dx \tag{107}$$

$$Q_{rad} = 1.065 \times 10^{14} \alpha exp\left(\frac{-141170}{T}\right)\left(\frac{W}{m^3}\right) \tag{108}$$

B Fullerene growth mechanism - short description

B.1 Kinetic models for C_{60}^{BF} production

Three major mechanisms for fullerene growth have so far been proposed. The first suggests the C_{60} is built up from intermediate sized clusters, the second favours minima energy path and the third proposes, that buckministerfullerens form from larger clusters by the addition of small clusters e.g C_2 and C_3.

B.1.1 Intermediate cluster formation

It was first believed that the fullerens were formed from napthalenic C_{10}, which first combines with C_{18} ring to form an open fullerene C_{28}. Another C_{18} ring is attached to C_{28}, followed by C_{12} and C_2 to reach C_{60}. Because of a high number of intermediate sized clusters observed in a carbon cluster distributions along with C_{60} it is unlikely that this approach is correct.

B.1.2 The pentagon road

The pentagon rule or the pentagon road assumes that fullerens are formed from energetically the most favoured form of an open graphitic sheet. In order to insure this criteria the following conditions known as the pentagon rule must be true: graphitic sheet is made up solely by pentagons and hexagons, it has as many pentagons as possible and it avoids adjacent pentagon units.

Graphite sheets are formed for cluster with more than 30 C atoms. Smaller C configurations are than ingested into the graphitic sheet. Since it is assumed that the process must follow the low energy path, pentagonal units are incorporated between the hexagonal ones. With the addition of pentagon units the sheet curls up and thus reduces the number of dangling bonds. The C_{60} is the first pentagon rule structure that is closed.

B.1.3 The fullerene road

The fullerene road suggests that fullerens form from clusters with more than 40 atoms and grow either by the addition of smaller carbon clusters or by opening and reclosing until they reach C_{60}. Odd clusters when formed are very reactive, which is why they are easily converted to fullerenes by loss or extraction of a C atom. The adjacent pentagon bonds are removed by ring rearrangement.

C Production techniques - short description

The most common techniques in fullerene and nanotube production today are arc-discharge method, chemical vapour deposition and laser vaporisation technique. The techniques vary in catalysts type, inert gas type, yield, purity and type of the material produced (fullerene, SWNT, MWNT). The cheapest and easiest method to obtain significant amount of material is arc-discharge method. However, this method requires separating the desired product from the soot and the catalytic particles that might be present in the crude product.

C.1 Arc-discharge method

C.1.1 Process description

Most common laboratory scale, carbon arc reactor consist of a typically water cooled chamber, which is filled with an inert gas, usually argon or helium. Two cooled graphite rods are placed in the enclosure and the distance between them is adjusted in order to to maintain a constant voltage between these electrodes. The anode is generally made of carbon and filed with catalysts (Co, Fe, Ni, Y, or the mixture of these elements) and the cathode is normally

made of pure graphite. A current that passes through electrodes creates plasma in the space between them. A direct current is used for nanotube production and an alternating current is used for fullerene production. The process starts at the contact point of the anode and the cathode. The electrodes are kept in contact until the current generated temperature is high enough to ignite the plasma and cause the anode material to evaporate. Carbon species and catalysts vapour that are produced in the hot plasma zone, build up a deposit on the cathode. By maintaining the desired gap between the growing deposit on the cathode and the burning anode we ensure that the anode erosion rate is constant and that the plasma, ignited between the cathodes, is stable. Efficient operation is assumed to exist in such conditions. Most of the anode material is vaporised due to high temperatures near the anode and high energy density in the plasma. Since the cathode is water-cooled, the quench at the edges of the electrode leads to high levels of super cool or supersaturated vapour in which fullerens and nanotubes are formed. The products of the arc discharge reactor are deposit on the cathode, rubber-like collaret around the cathode deposit, web-like structures between the cathode and reactor walls and soot on the reactor walls.

Fullerenes are formed outside the inner electrode gap and are found in the soot on the reactor walls, multi-walled carbon nanotubes (MWNT) are formed only in the inter-electrode gap where the current is flowing and thus require a maximization of cathode deposit, whereas single-wall carbon nanotubes (SWNT) are found in the collaret. The abundance of carbon forms is strongly dependent on the input power, the current applied on the electrodes, the distance between the electrodes, their cooling, the chemical composition of the anode, the nature and the pressure of the inert gas, the temperature of plasma, the energy transfer and the geometry of the reactor.

C.2 Alternative techniques

C.2.1 Laser ablation (vaporisation) method

Laser ablation method uses pulsed or continuous laser to vaporise graphite from a target placed in an oven. The oven is filled with inert gas (usually argon or helium) at high temperature. Vaporised atoms and molecules condense into bigger clusters to form fullerens or nanotubes. The process and conditions in which material is formed are very similar to the arc-discharge method.

C.2.2 Chemical vapour deposition (CVD) method

In CVD method nanotubes are synthesised from hydrocarbon vapour decomposition, which is in direct contact with catalytic particle. The furnace tube, where catalytic material is kept, is heated to the growth temperature, at which point the carbon feedstock is introduced. As

the carbon diffuses toward the metal catalysts, it binds with it and nanotubes are formed. This method is used primary for nanotube synthesis.

References

[1] J-F. Bilodeau, J. Pousse, A. Gleizes, *A mathematical model of the carbon arc reactor for fullerene synthesis*. Plasma Chem. and Plasma Process. 18 (1998) 285-303

[2] S. Farhat, C. D. Scott, *Review of the Arc Process Modeling for Fullerene and Nanotube Production* J. Nanosci. Nanotechnol. 6 (2006) 1189-1210

[3] N.I. Alekseyev, G.A. Dyuzhev, *Evolution of carbon from atomic clusters to fullerenes in an arc discharge*. Tech. Phys. 47 (2002) 634-642. Translated from Zh. Tekh. Fiz. 72 (2002) 121129

[4] N. Grlj, *Fullerene production with electric arc-discharge method*. Seminar.

[5] H.W. Kroto, J.R. Heath, S.C. O'Brian, R.F. Curl, R.E. Smalley, C_{60}*: Buckminsterfullerene*. Nature 318 (1985) 162-163

[6] S. Iijima. Nature 354, 56 (1991)

[7] S. Iijima and T. Ichihashi. Nature 363, 603 (1993)

[8] D. S: Bethune, C. H. Kiang, M. S. DeVries, G. Gorman, R. Savoy, J. Vazquez, and R. Beyers. Nature 363, 605 (1993)

[9] W. Kratschmer, L.D. Lamb, K. Fostiropoulos, D.R. Huffmann, *Solid* C_{60}*: a new form of carbon*. Nature 347 (1990) 354-357

[10] G.N. Churilov, P.V. Novikov, V.E. Tarabanko, V.A. Lopatin, N.G. Vnukova, N.V. Bulina, *On the mechanism of fullerene formation in a carbon plasma*. Carbon 40 (2002) 891896

[11] C. D. Scott, *Chemical Models for Simulating Single-Walled Nanotube Production in Arc Vaporisation and Laser Ablation Processes* J. Nanosci. Nanotechnol. 4 (2004) 368-376

[12] R. Vertnik, *Heat and Fluid Flow simulation of the continuous casting of steel by a meshless method* (2010)

[13] $http://www.theorie2.physik.uni-erlangen.de/collaboration/intro.html$. 4.1.2011

[14] $http://en.wikipedia.org/wiki/Carbon_nanotube$. 4.1.2011

[15] $http://www.3rd1000.com/bucky/bucky.htm$. 3.1.2011

[16] $http://www.hanwhananotech.com/WebContent/pro/$. 30.12.2011

[17] *http : //www.istockphoto.com/stock − photo − 9644738 − multi − walled − carbon − nanotubes.php*. 30.12.2011

[18] *http : //en.wikipedia.org/wiki/Soxhlet$_e$xtractor*. 20.1.2011

[19] *http : //www.nanowerk.com/spotlight/spotid = 841.php*. 20.1.2011

[20] L. Chow, H. Wang, S. Kleckley, T.K. Daly, P.R. Buseck, *Fullerene formation during production of chemical vapor deposited diamond*. Appl. Phys. Lett. 66 (1995) 430-432

[21] S.H. Jung, M.R. Kim, S.H. Jeong, S.U. Kim, O.J. Lee, K.H. Lee, J.H. Suh, C.K. Park, *High-yield synthesis of multi-walled carbon nanotubes by arc discharge in liquid nitrogen*. Appl. Phys. A 76 (2003) 285286

[22] A. Hirsch, M. Brettreich, *Fullerenes: Chemistry and reactions*. Wiley-VCH, Weinheim, 2005

[23] Y. Saito, M. Inagaki, H. Shinohara, H. Nagashima, M. Ohkohchi, Y. Ando, *Yield of fullerenes generated by contact arc method under He and Ar: dependence on gas pressure*. Chem. Phys. Lett. 200 (1992) 643-648

[24] A. Weston, M. Murthy, *Synthesis of fullerenes: an effort to optimize process parameters*. Carbon 34 (1996) 1267-1274

[25] A. Huczko, H. Lange, Byszewski, *Control of fullerene generation through the macroscopic parameters of carbon plasma arc*. Full. Sci. and Technol. 4 (1996) 385-397

[26] A. Huczko, H. Lange, P. Byszewski, M. Poplawska, A. Starski, *Fullerene Formation in Carbon Arc: Electrode Gap Dependence and Plasma Spectroscopy*. J. Phys. Chem. A 101 (1997) 1267-1269

[27] Z.M. Marković, T.Lj. Joki, B.M. Todorovi-Marković, J.L. Blanua, T.M. Nenadovi, *Model of improved arc generator for fullerene production*. Full. Sci. and Technol. 5 (1997) 903-918

[28] A.V. Krestinin, A.P. Moravsky, *Mechanism of fullerene synthesis in the arc reactor*. Chem. Phys. Lett. 286 (1998) 479-484

[29] A.V. Krestinin, A.P. Moravsky, *Kinetics of fullerene* C_{60} *and* C_{70} *formation in a reactor with graphite rods evaporated in electric arc*. Chem. Phys. Reports 18 (1999) 515-532

[30] T. Sugai, H. Omote, S. Bandow, N. Tanaka, H. Shinoharac, *Production of fullerenes and single-wall carbon nanotubes by high-temperature pulsed arc discharge*. J. Chem. Phys. 112 (2000) 6000-6005

[31] Z. Marković, B. Todorovi-Marković, M. Marinkovi, T. Nenadovi, *Temperature measurement of carbon arc plasma in helium*. Carbon 41 (2003) 369384

[32] R. Dubrovsky, V. Bezmelnitsyn, Yu. Sokolov, *Reduction of cathode carbon deposit by buffer gas outflow*. Carbon 43 (2005) 796802

[33] X. Song, Y. Liu, J. Zhu, *The effect of furnace temperature on fullerene yield by a temperature controlled arc discharge*. Carbon 44 (2006) 15811616

[34] K. Saidane, M. Razafinimanana, H. Lange, A. Huczko, M. Baltas, A. Gleizes, J-L. Meunier, *Fullerene synthesis in the graphite electrode arc process: local plasma characteristics and correlation with yield*. J. Phys. D: Appl. Phys. 37 (2004) 232-239

[35] G. Meijer, D.S. Bethune, *Laser deposition of carbon clusters on surfaces: A new approach to the study of fullerenes*. J. Chem. Phys. 93 (1990) 7800-7802

[36] T.W. Ebbensen, J. Tabuchi, K. Tanigaki, *The mechanistics of fullerene formation*. Chem. Phys. Lett. 191 (1992) 336-338

[37] N.S. Goroff, *Mechanism of fullerene formation*. Acc. Chem. Res. 29 (1996) 77-83

[38] Z.M. Marković, B.M. Todorovi-Marković, T.Lj. Joki, P. Pavlovi, P. Stefanovi, J.L. Blanua, T.M. Nenadovi, *Kinetics of fullerene formation in a contact arc generator*. Full. Sci. and Technol. 6 (1998) 1057-1068

[39] G.N. Abramovich, *Prikladnaya Gazovaya Dinamika (Applied Gas dynamics)*. Nauka, Moscow, 1969

[40] N.I. Alekseyev, G.A. Dyuzhev, *Production of fullerenes in gas discharge plasmas. I. Kinetics of fullerene formation from polycyclic structures*. Tech. Phys. 44 (1999) 1093-1097. Translated from Zh. Tekh. Fiz. 69 (1999) 104109

[41] N.I. Alekseyev, G.A. Dyuzhev, *A statistical model of fullerene formation based on quantum-chemistry calculations. The most probable precursors of fullerenes, verification of the model and kinetics of transformation into fullerene*. Tech. Phys. 46 (2001) 573-583.

[42] N.I. Alekseyev, G.A. Dyuzhev, *On the transformation of carbon vapor in the gas-plasma jet of an arc discharge*. Tech. Phys. 46 (2001) 761-766. Translated from Zh. Tekh. Fiz. 71 (2001) 122126

[43] N.I. Alekseyev, G.A. Dyuzhev, *Analysis of an arc-formed gas-plasma jet in the arc method for fullerene production*. Tech. Phys. 50 (2005) 1423-1430. Translated from Zh. Tekh. Fiz. 75 (2005) 3239

[44] N.I. Alekseyev, G.A. Dyuzhev, *Fullerene formation in an arc discharge*. Carbon 41 (2003) 1343-1348

[45] A. Dudek, Z. Nitkiewicz, *Diagnostics of plasma arc during the process of remelting of surface layer in 40r4 steel* Archives of Material Sci. and Eng. 28 (2007) 369-372

[46] I. Hinkov, S. Farhat, C. D. Scott, *Influence of the gas pressure on single-wall carbon nanotube formation*. Carbon 43 (2005) 2453-2462

[47] M. tanaka, M. Ushio, J.J. Lowke, *Numerical study of gas tungsten arc plasma with anode melting*. Vacuum 73 (2004) 381-389

[48] M.E. Coltrin et. all, *SPIN (Version 3.83): A Fortran Program for Modeling One-Dimensional Rotating-Disk/Stagnation-Flow Chemical Vapor Deposition Reactors*. (1991)

[49] G. Kosec, B. Šarler, *Solution of thermo-fluid problems by collocation with local pressure correction*. J. Num. Meth. Heat and Fluid Flow 18 (2008) 868-882

[50] B. Šarler, R. Vertnik, *Meshfree explicit radial basis function collocation method for diffusion problems*. Computers and Mathematics with Application 51 (2006) 1269-1282

[51] R. J. Kee et al, *CHEMKIN Collection*. Release 3.6, Reaction Design, Inc. San Diego, CA.(2001)

[52] L. V. Gurvich et al, *IVTANTHERMO, User's guide*. CRC Press, Inc. Boca Raton. (1993)

[53] G. Kosec, *LOCAL MESHLESS METHOD FOR MULTI-PHASE THERMO-FLUID PROBLEMS*. (2011)